

Longevity Studies on the CDFII Silicon Detectors

Benedetto Di Ruzza on behalf of the CDF II Silicon Operation Group



**4th National Course “Detectors and Electronics for High Energy physics,
Astrophysics, Space and Medical physics”**

INFN National Laboratories of Legnaro (Italy) April 11th – 15th 2011

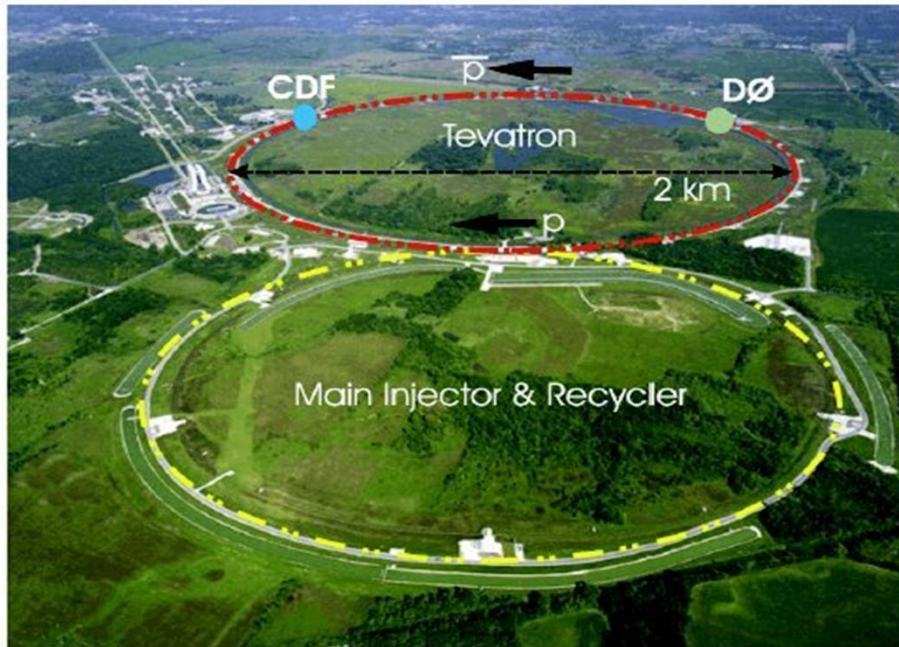


OUTLINE

- 1) The Tevatron
- 2) The CDF II detector
- 3) The CDF II silicon subdetectors
- 4) Silicon aging studies
- 5) Conclusions



The Tevatron



➤ **Tevatron:** proton-antiproton collider
at $\sqrt{s} = 1.96 \text{ TeV}$

Luminosity: more than **8 fb^{-1}** delivered

Expected **11 fb^{-1}** delivered by 2011

Two multi-purpose detectors: CDF & DØ

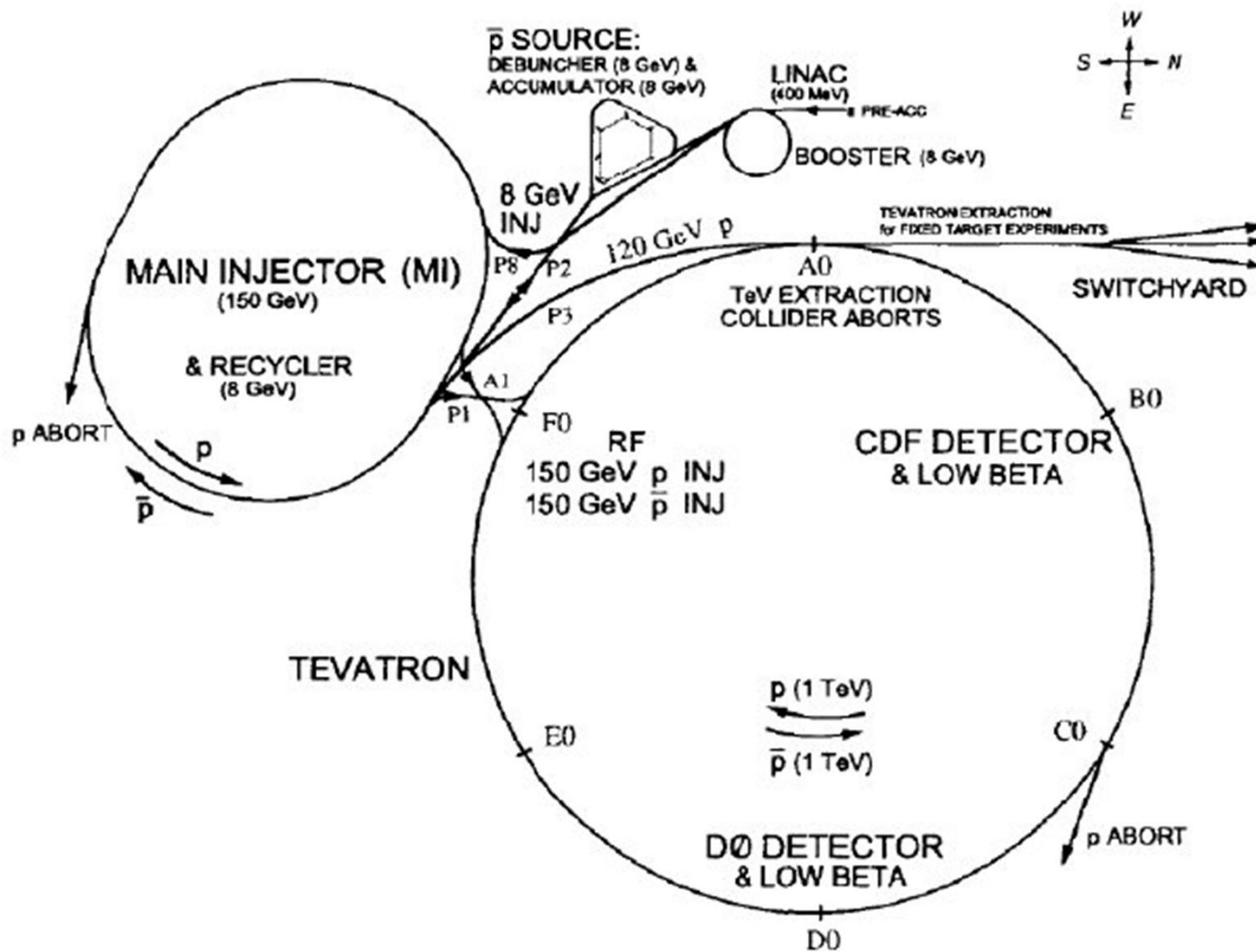
➤ **CDF II:** Multilayered HEP detector
with **excellent tracking**

✓ silicon detectors designed for **$\sim 3 \text{ fb}^{-1}$**

✓ large open-cell drift chamber



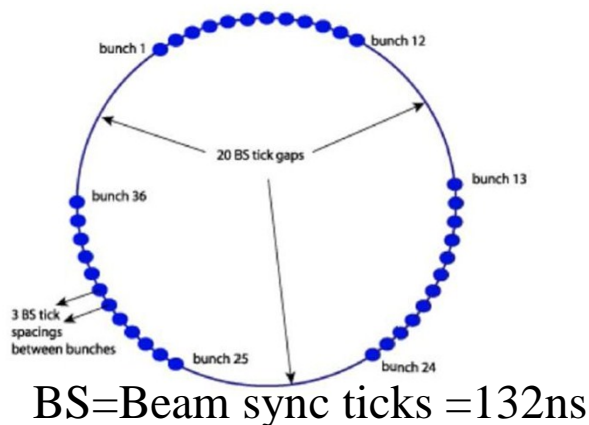
Fermilab accelerators chain





The Tevatron

Bunches structure

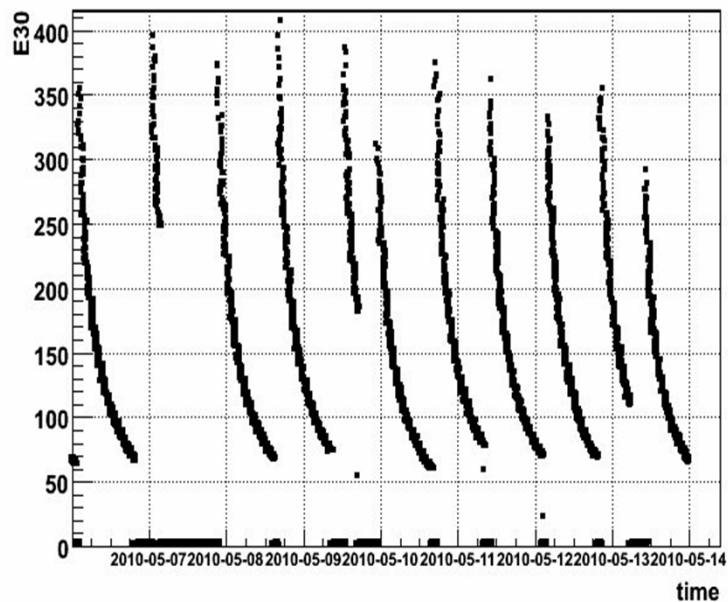


Initial luminosity record: $4.02 \times 10^{32} \text{ (cm}^{-2} \text{ s}^{-1})$

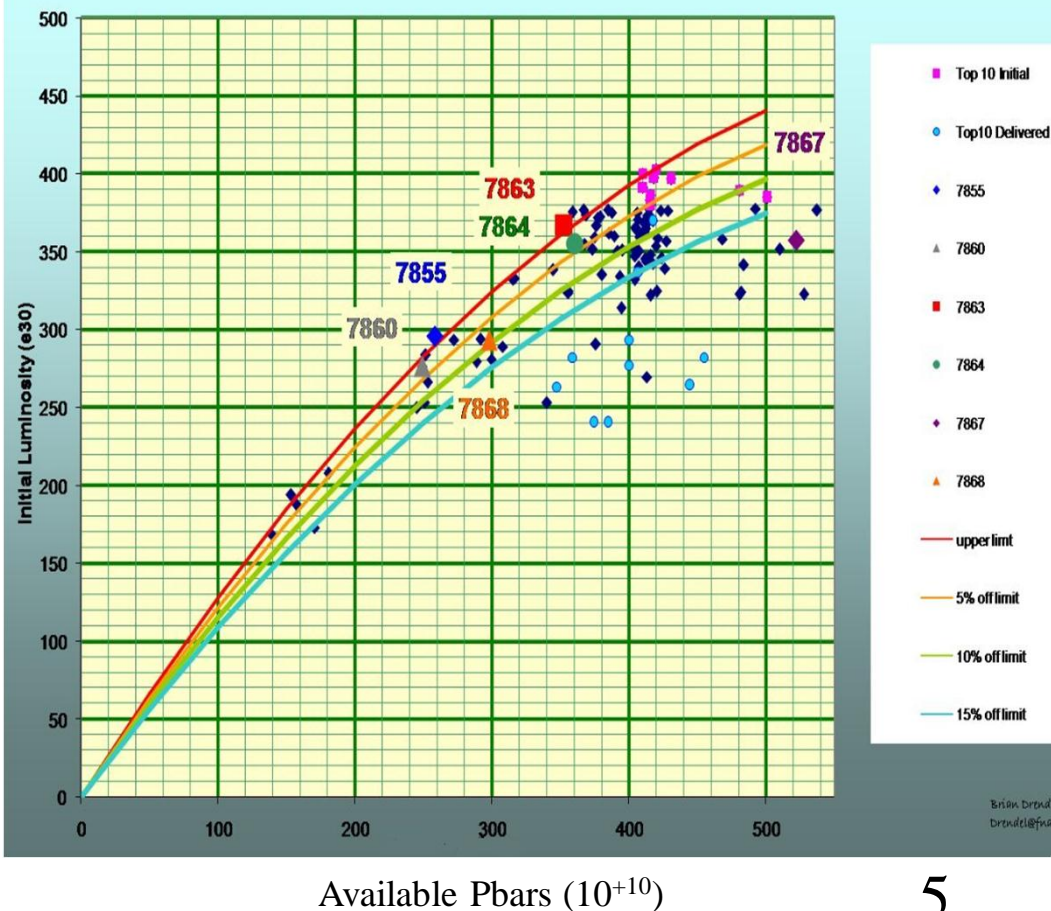
Mean Pbar production efficiency: $\sim 22 \times 10^{-6}$

Mean Pbar Accumulation rate: $\sim 25 \times 10^{10} \text{ (hr}^{-1})$

B0ILUM_2010.05.06:00:00_to_2010.05.14:00:00 Entries 5760



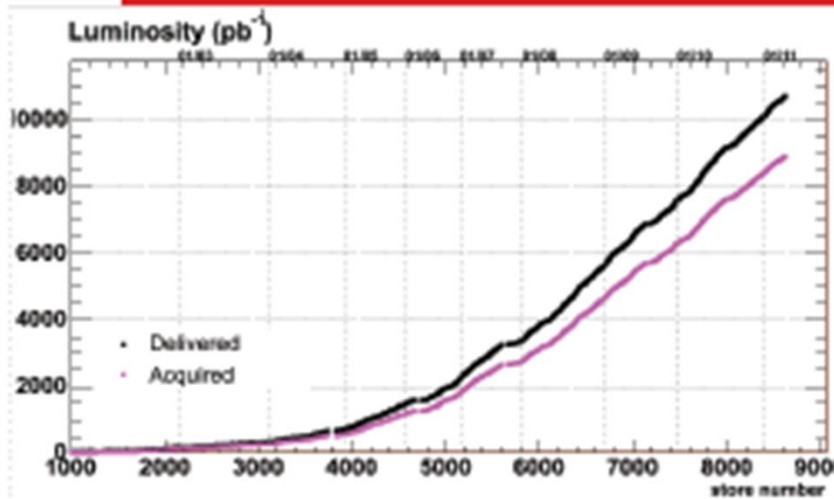
Average Initial Luminosity vs Available Pbars





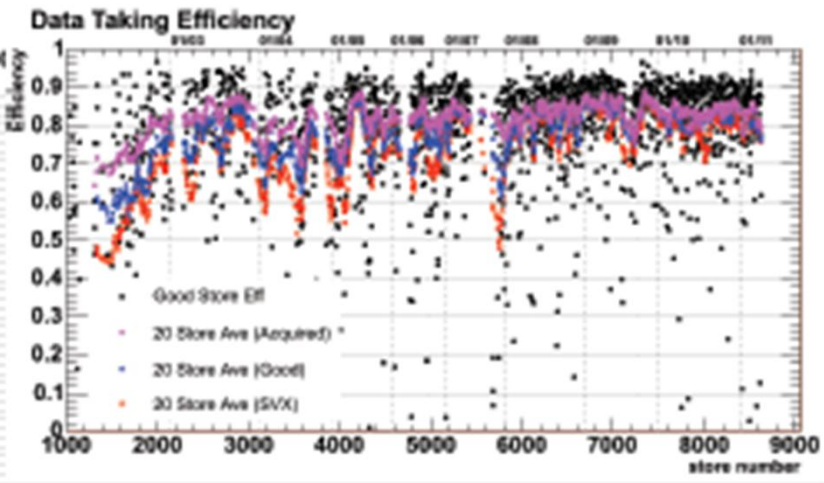
Tevatron Luminosity

Grand Summary



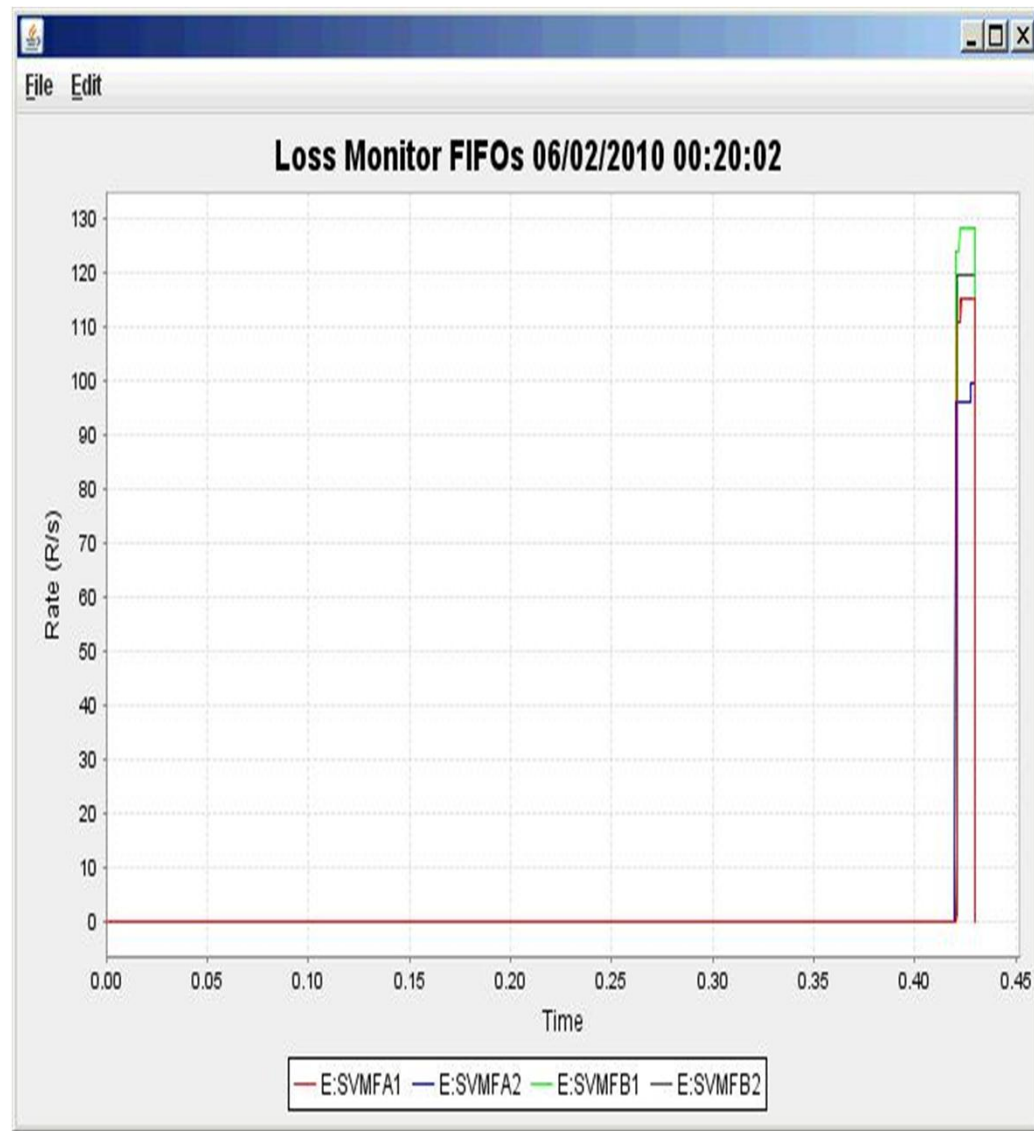
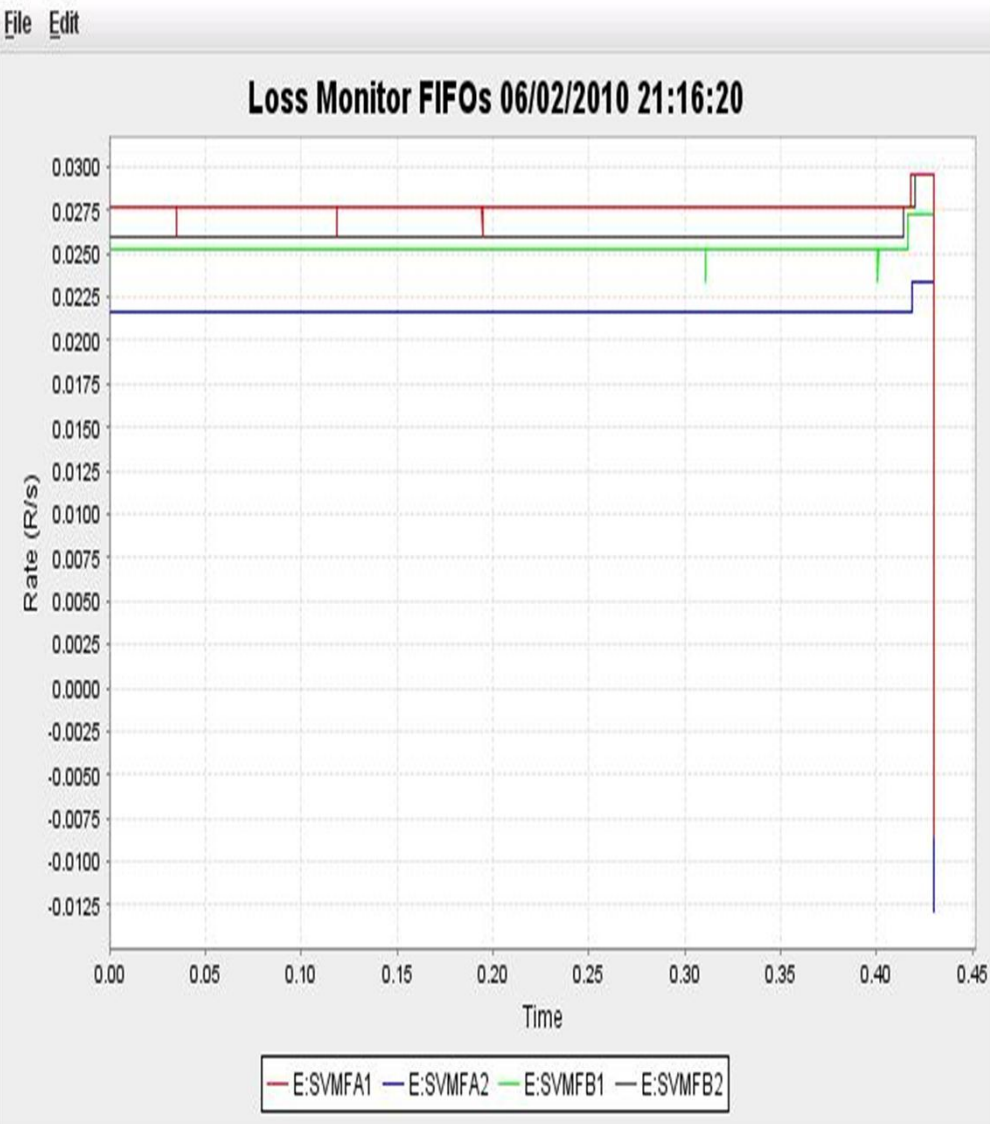
Delivered: 10,685.1 pb^{-1}
Acquired: 8,887.3 pb^{-1}

Efficiency: 83.2%



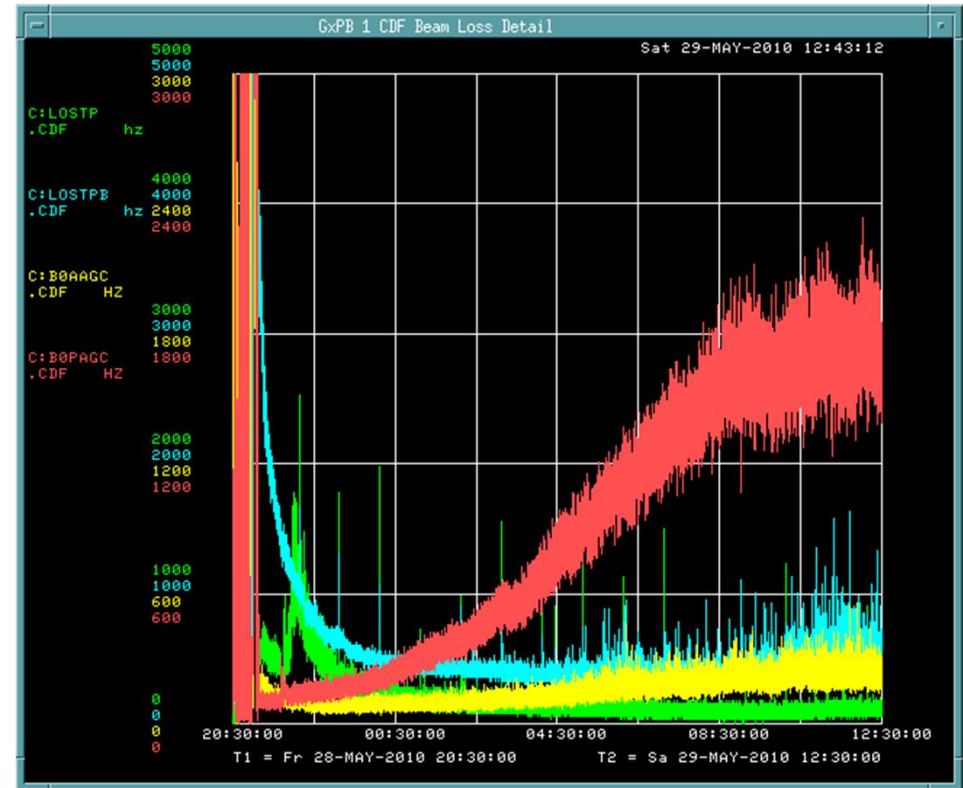
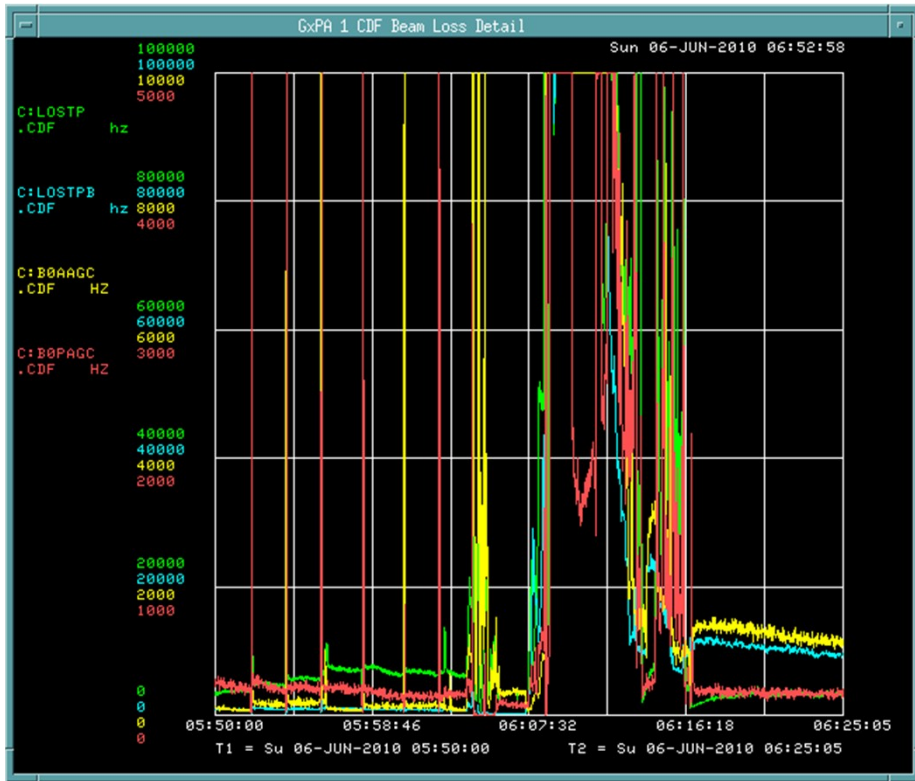


Dose during beam dump



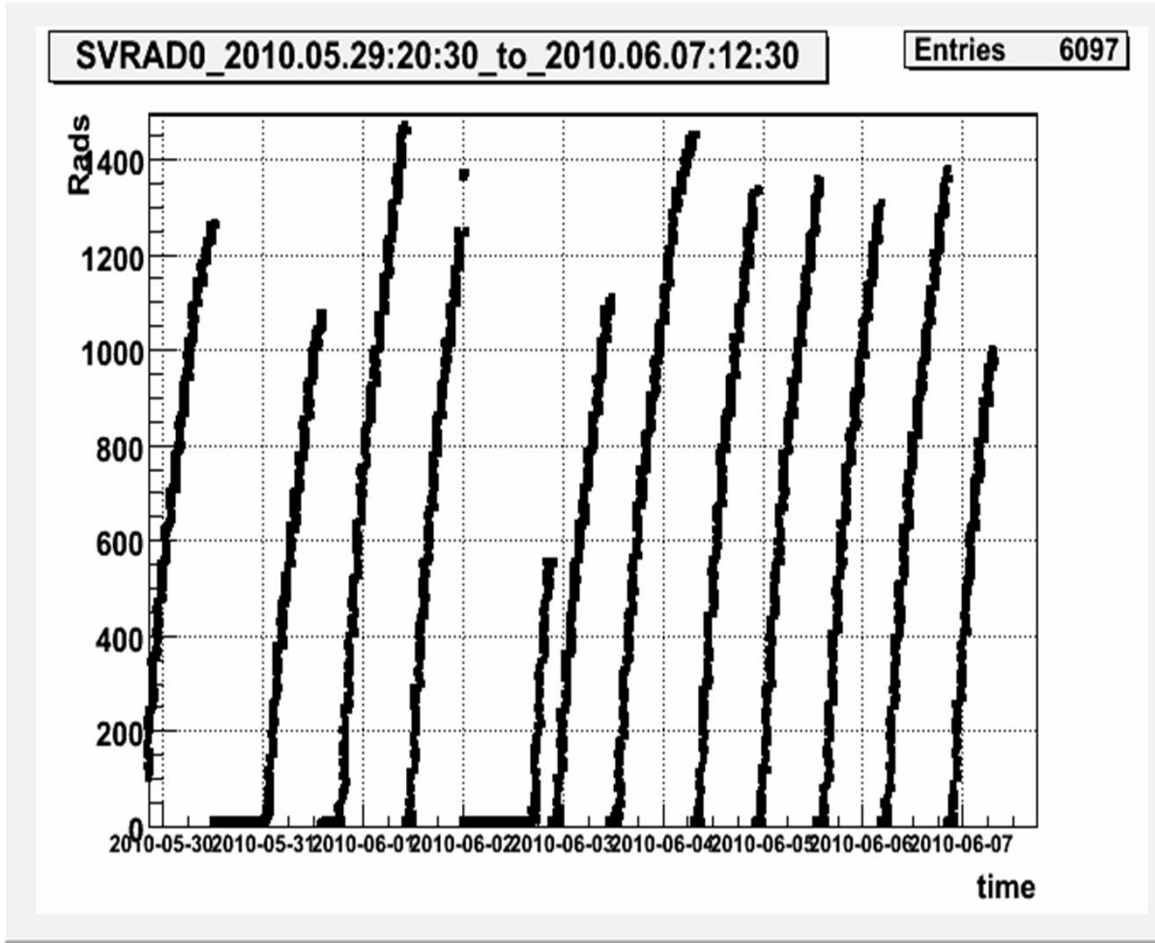
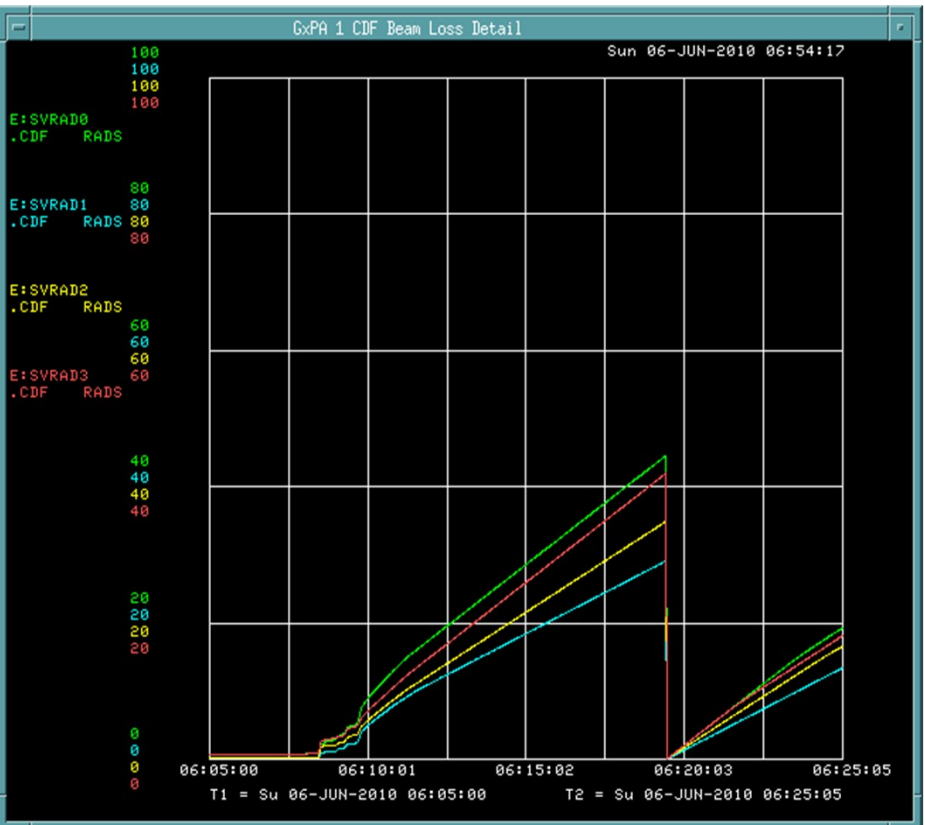


Beam condition



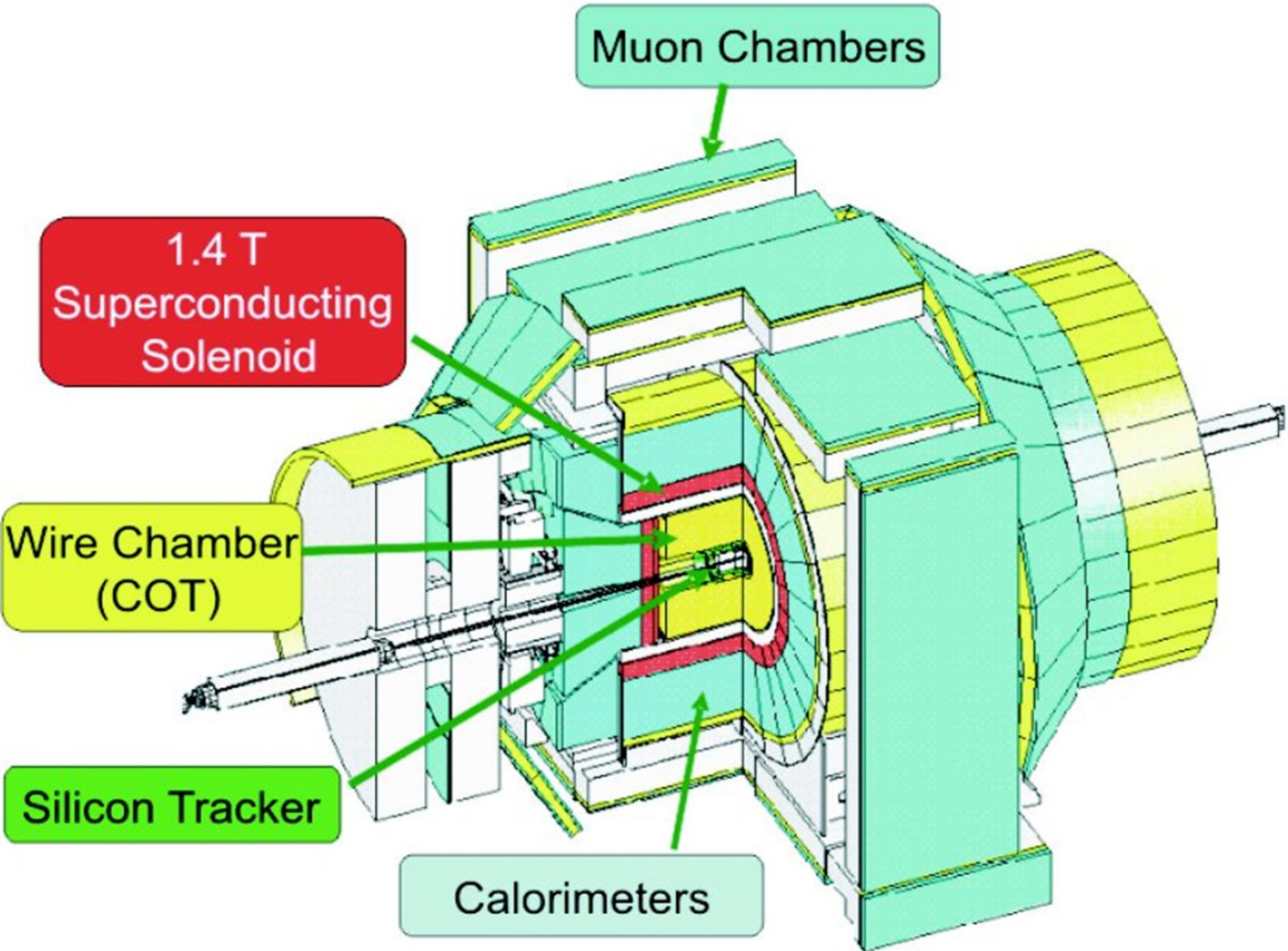


Beam doses





The CDFII Detector





The CDFII Silicon detectors

Overview:

- ✓ Three components: **SVX-II, ISL, L00**
- ✓ 7-8 layers, 722k readout channels
- ✓ 3D hit information
- ✓ Forward tracking with ISL and improved vertexing with L00
- ✓ **SVX3** chips for the silicon readout

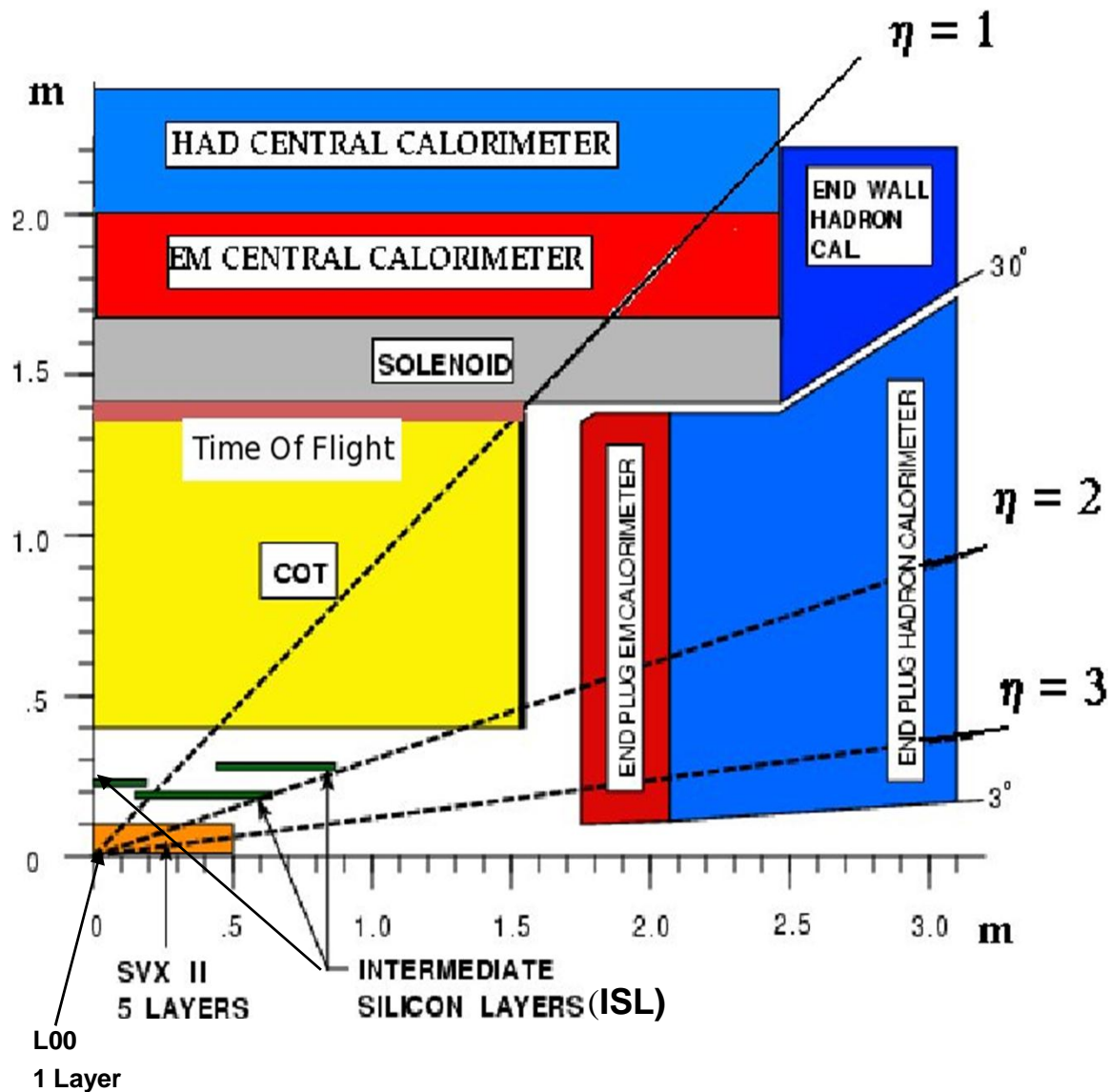
L00: Single-sided strips: “Narrows” (SGS Thomson and 2 Microns)
“Wides” (Hamamatsu).

SVX: Double-sided strips: Layers 0,1,3 (Hamamatsu) **perpendicular strips**,
Layers 2,4 (Micron) **small angled strips**.

ISL: Double-sided strips: (Hamamatsu+Micron) **small angled strips**

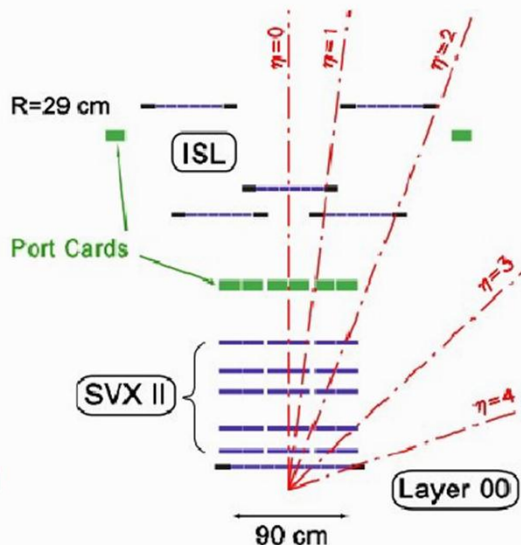
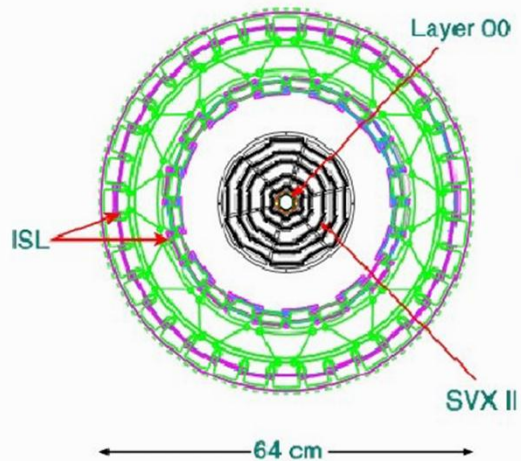


The Silicon Detectors



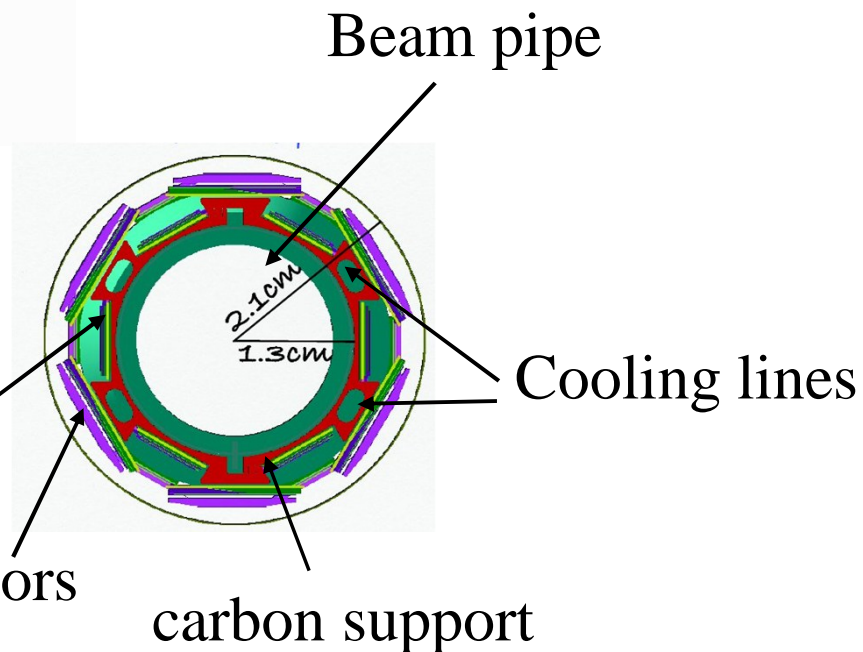


The Silicon Detectors



←== X-Y (r-phi) and Y-Z (r-z) views

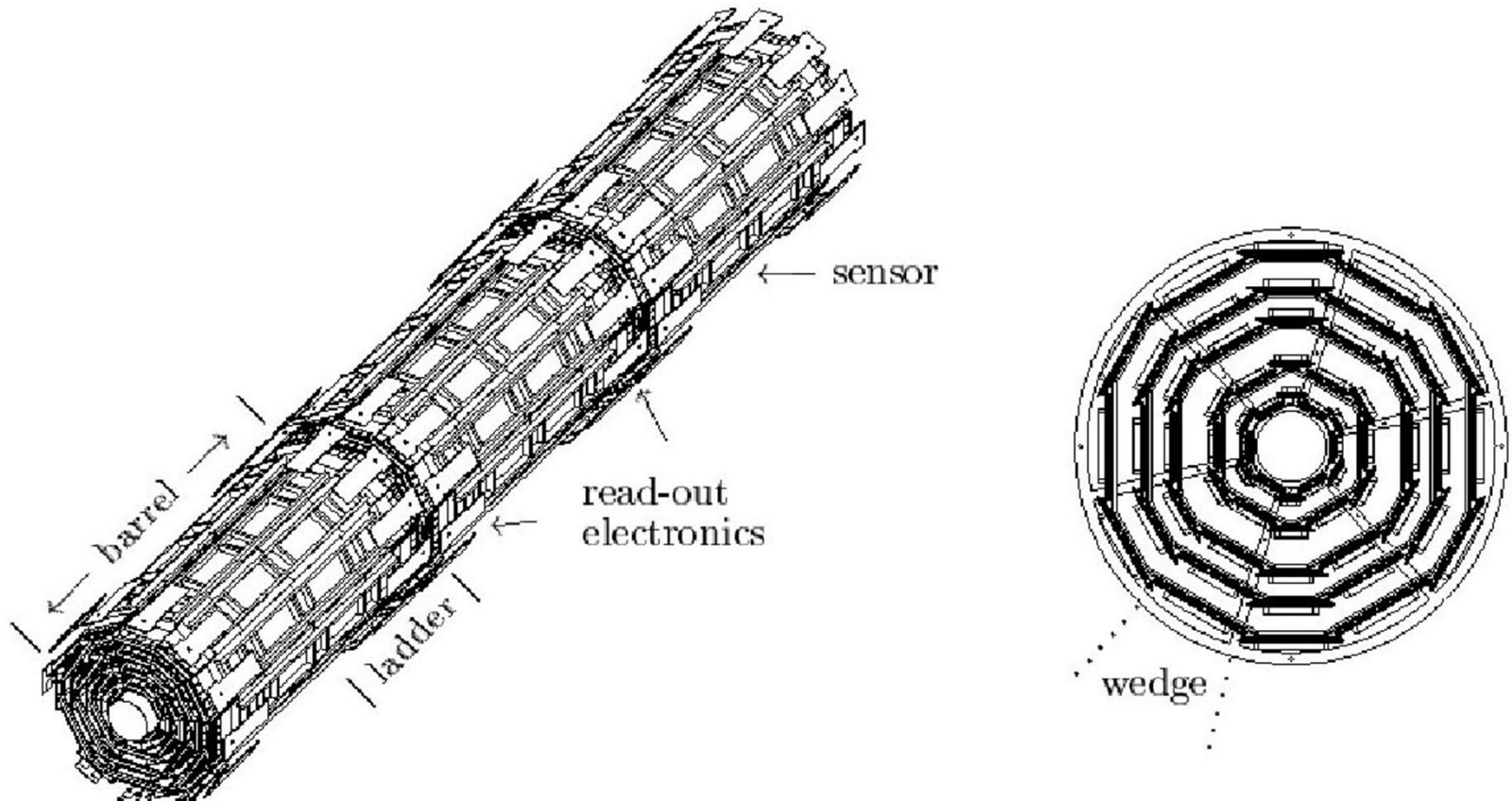
L00 detail ==> narrow sensors





The Silicon Detectors

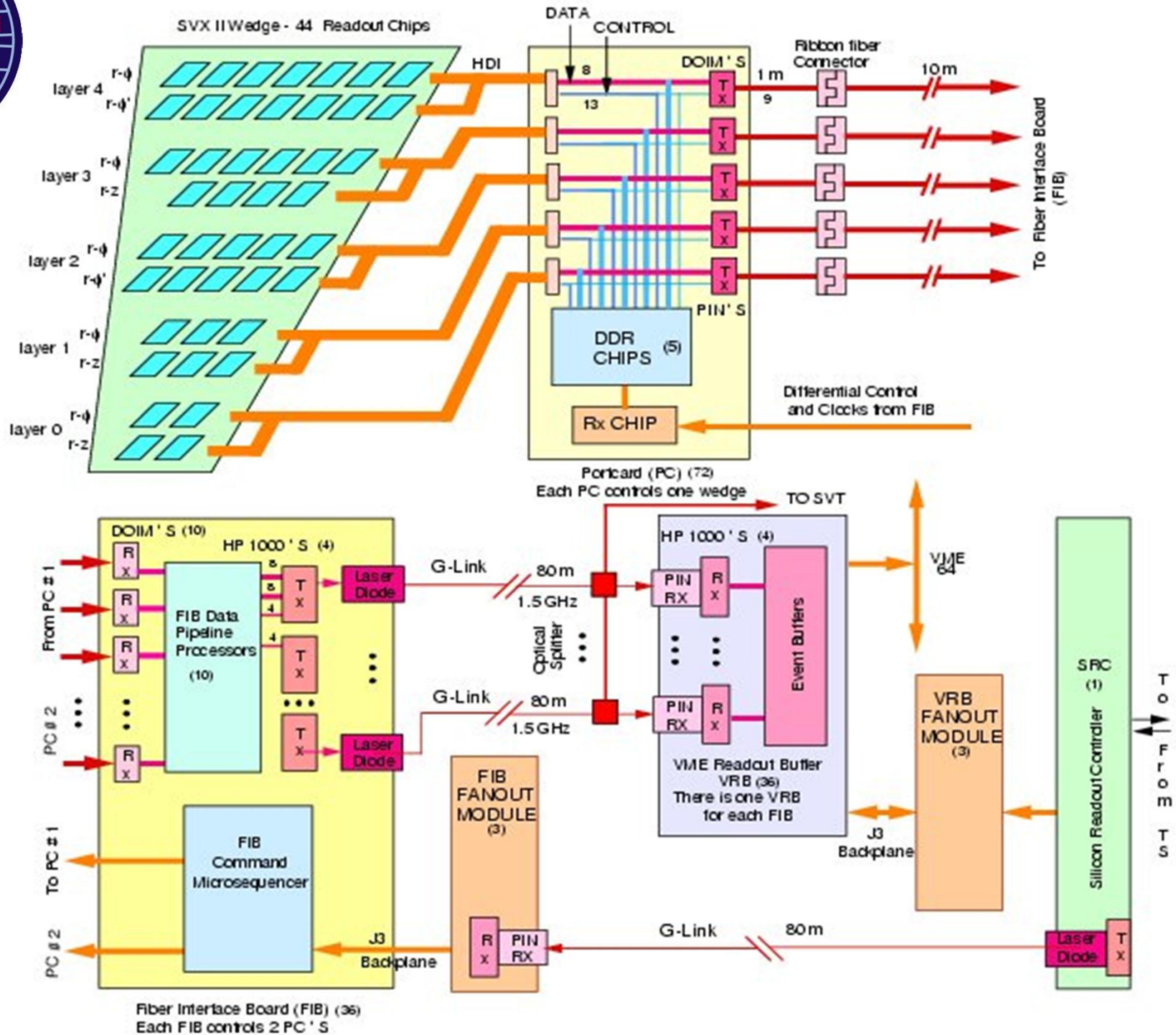
SVXII detail:
3 barrels
5 layers
12 wedges



SVXII: the readout is
used in the trigger too



Silicon D.A.Q. for SVX II





SVXII.

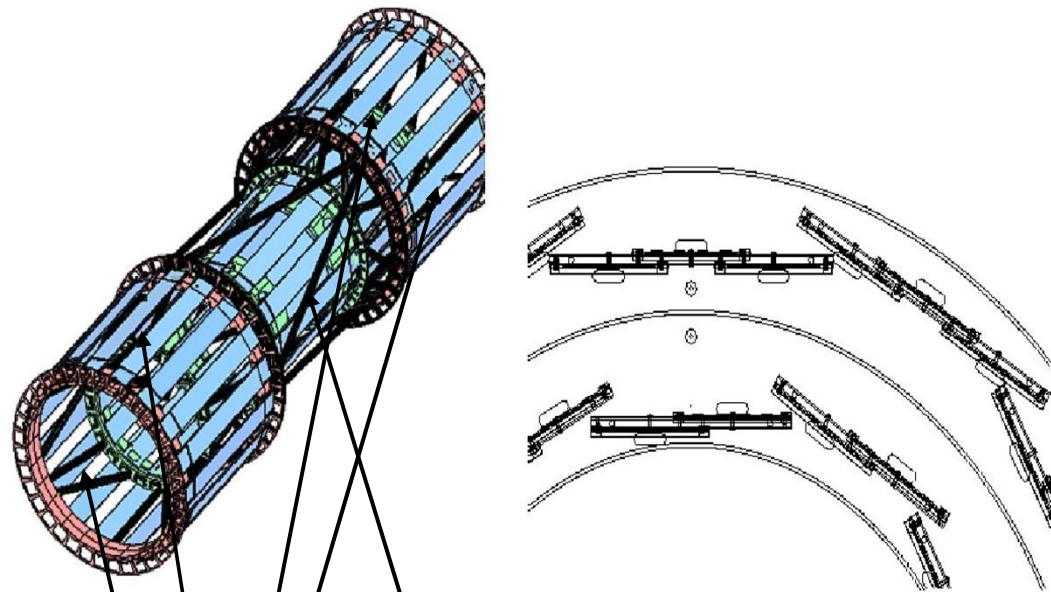
| Property | Layer 0 | Layer 1 | Layer 2 | Layer 3 | Layer 4 |
|--------------------------------|------------|------------|--------------|------------|--------------|
| number of ϕ strips | 256 | 384 | 640 | 768 | 896 |
| number of Z strips | 256 | 576 | 640 | 512 | 896 |
| number of ϕ chips | 2 | 3 | 5 | 6 | 7 |
| number of Z chips | 2 | 3 | 5 | 4 | 7 |
| stereo angle | 90° | 90° | $+1.2^\circ$ | 90° | -1.2° |
| ϕ strip pitch (μm) | 60 | 62 | 60 | 60 | 65 |
| Z strip pitch (μm) | 141 | 125.5 | 60 | 141 | 65 |
| total width (mm) | 17.140 | 25.594 | 40.300 | 47.860 | 60.170 |
| total length (mm) | 74.3 | 74.3 | 74.3 | 74.3 | 74.3 |
| active width (mm) | 15.300 | 23.746 | 38.340 | 46.020 | 58.175 |
| active length (mm) | 72.43 | 72.43 | 72.38 | 72.43 | 72.38 |
| number of detectors | 144 | 144 | 144 | 144 | 144 |

Table 5.3: Silicon detector mechanical dimensions



The Silicon Detectors: ISL

ISL detail



ISL central

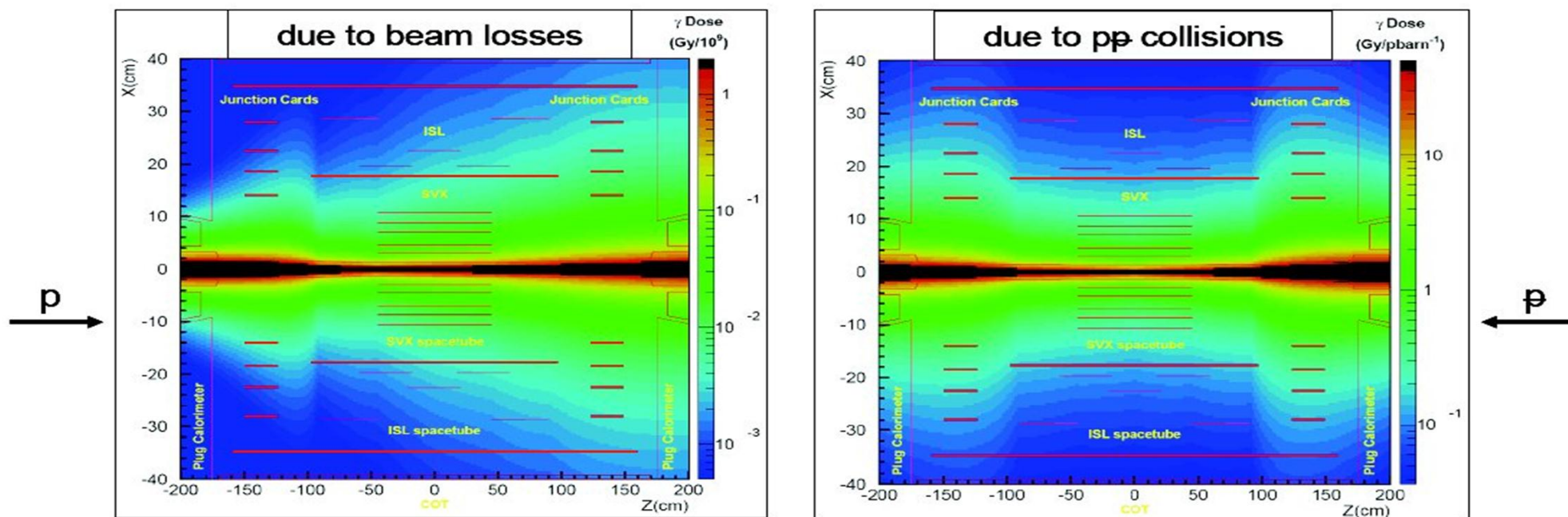
ISLforward:
(inner and external barrels)



Radiation Field inside the detector

CDF Radiation Field

- Measured using more than 1000 thermo-luminescent dosimeters (TLDs)



(See R. J. Tesarek *et al.*, IEEE NSS 2003)

- Radiation field is collision-dominated (> 90%) and scales with radius:

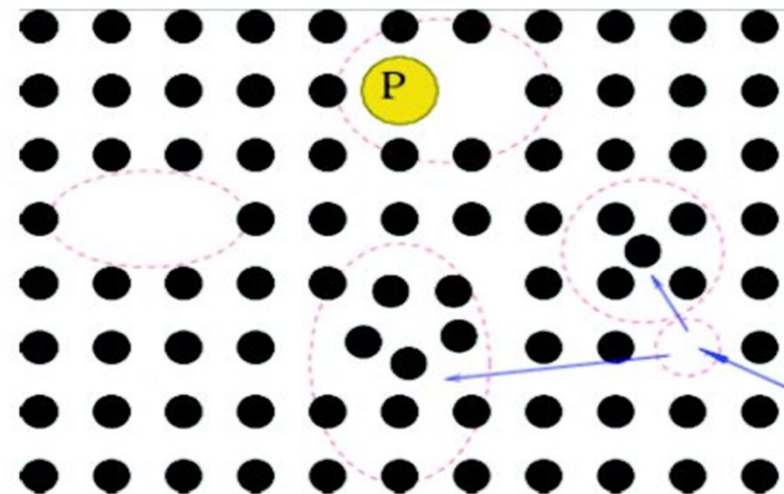
$$r^{-\alpha(z)}, \text{ with } 1.5 < \alpha(z) < 2.1$$
- Ionizing radiation dose at $r = 3 \text{ cm}$, $|z| < 45 \text{ cm}$: $300 \pm 60 \text{ kRad} / \text{fb}^{-1}$
- Use fluence conversion, $1 \text{ rad} = 3.87 \times 10^7 \text{ MIPs/cm}^2$, to predict integrated dose



Radiation damage

➤ Two general types of radiation damage to the sensors:

- **Crystal damage** due to Non-Ionizing Energy Loss (NIEL): displacement damage, crystal defects.
 - increase of shot noise, change of effective doping concentration, increase of charge carrier trapping.
- **Surface damage** from Ionizing Energy Loss (IEL) causing accumulation of charge in the SiO₂ and the Si/SiO₂ interface.
 - Inter-strip capacitance, breakdown behavior etc.



Crystal damage to the sensors is the main concern for detector longevity



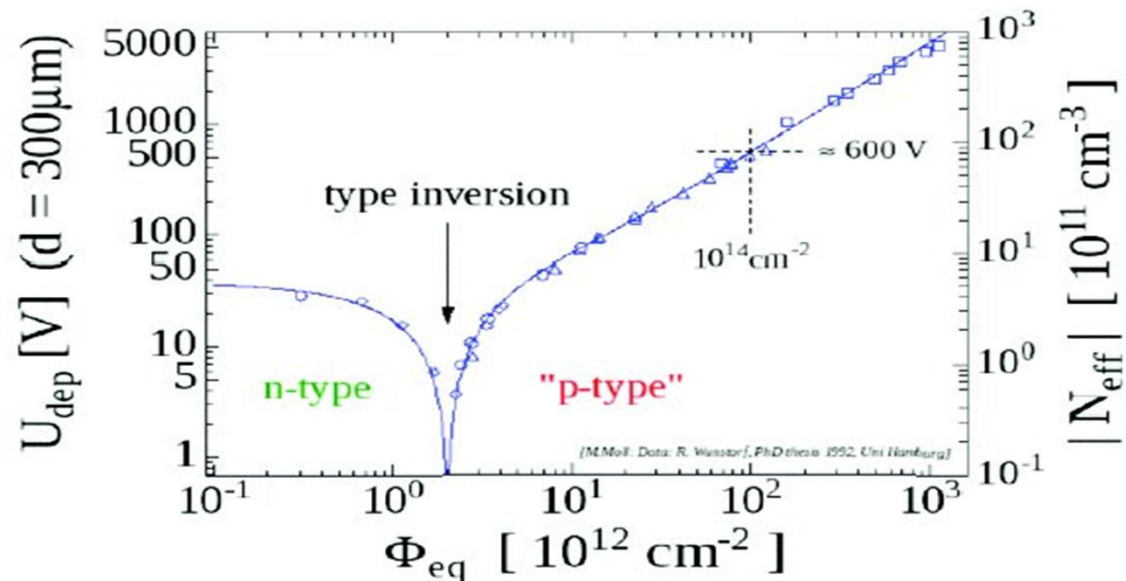
Aging studies: variables of interest

- Information on integrated radiation dose in a sensor is obtained from:
 - ✓ **evolution of bias current:** provides “direct” information on the crystal condition, due to increase in **leakage current**. Change in leakage current is linear with the absorbed dose $\Delta I_{\text{leak}} = \alpha \Delta \Phi_{\text{eq}}$ (α measured in 2004 to be **1.65 ± 0.12**)
 - ✓ **evolution of depletion voltage:** gives information on our ability to deplete the sensors in the future. Its extrapolation predicts the need to raise applied bias voltage and its limit.
 - ✓ **Signal-over-noise (S/N) studies:** provide estimates of usability of the detector in charged particle tracking and in turn for physics analyses.



Depletion Voltage

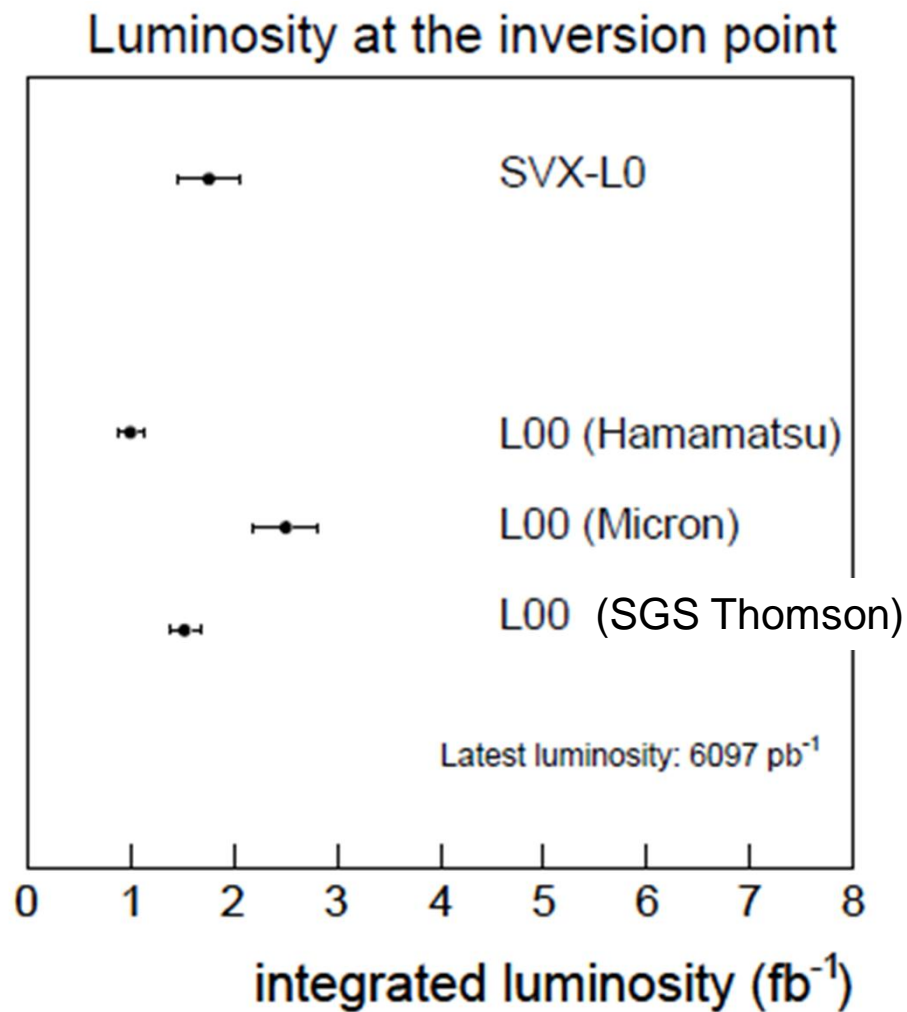
- Depletion voltage is the bias voltage required to get rid of free carriers in the bulk of the detector.
- The expected evolution depends on the dose (**Hamburg Model**):
- Before type inversion the depletion voltage decreases due to the reduction in the amount of free carriers
- After type inversion, depletion voltage steadily increases.



Sensor can operate while the Bias Voltage is below the Breaking Voltage



Inversion point





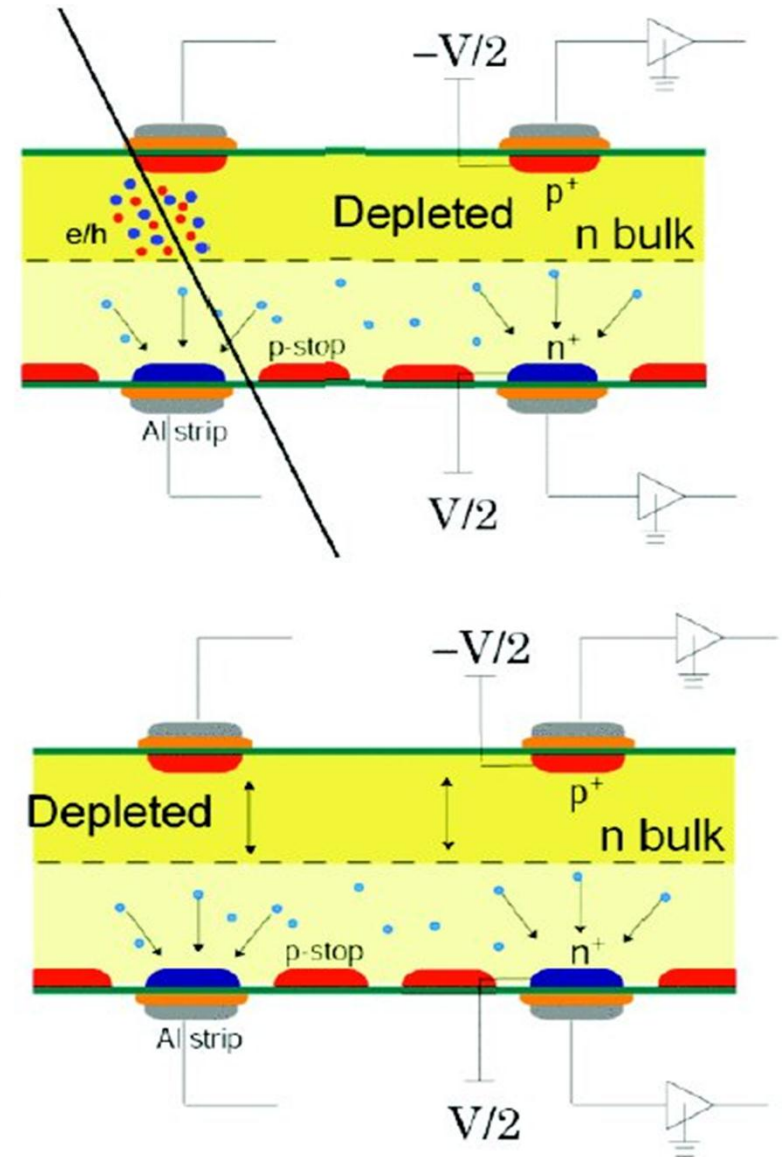
Depletion voltage Measurement

➤ From charge (signal) collection efficiency:

- Charge collection is proportional to the depleted volume
- Fully depleted sensor → charge collection efficiency saturates
- Extracted track residual information

➤ From noise at the n-side:

- Thermal noise from free carriers on the n-side is reduced with depletion (on the p-side)



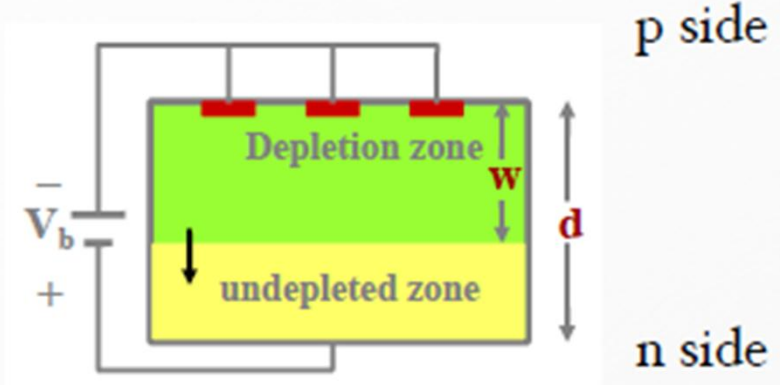
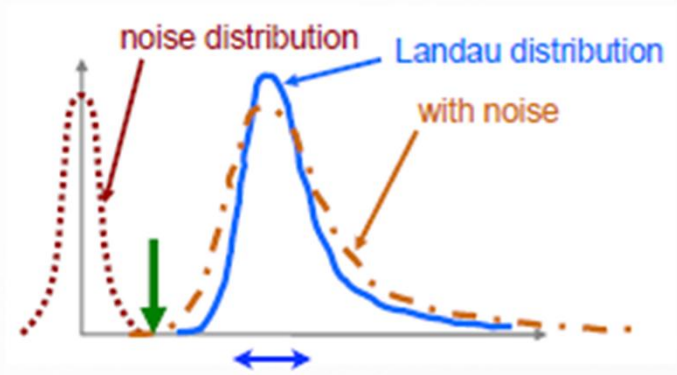


Depletion Voltage

Bias Scan Methods

Vary bias voltage and watch

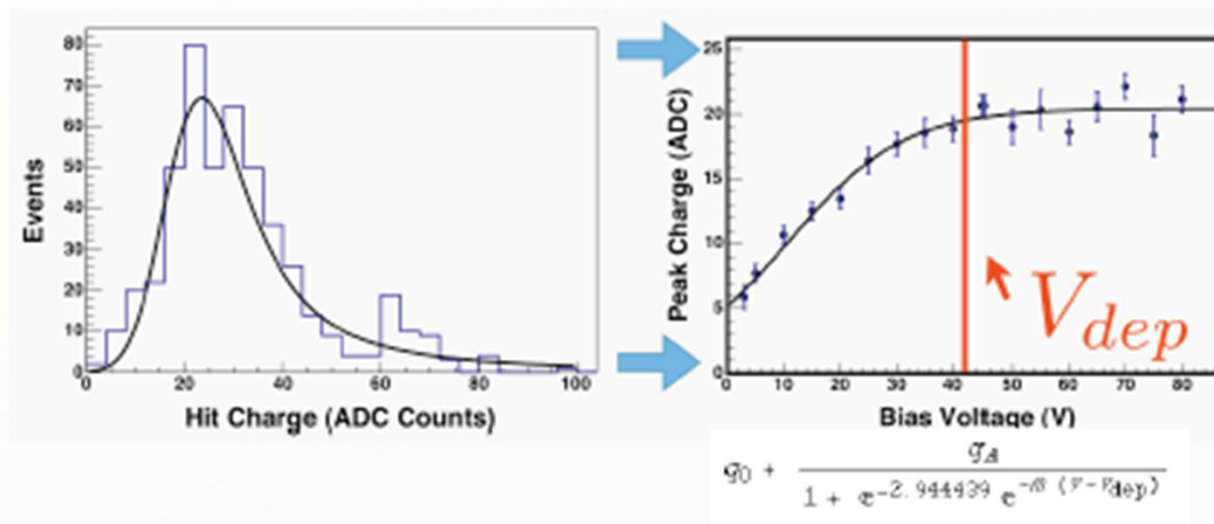
- signal collection
- dnoise from n side strips





Depletion Voltage study – Signal Vs. Bias

Signal vs Bias Method

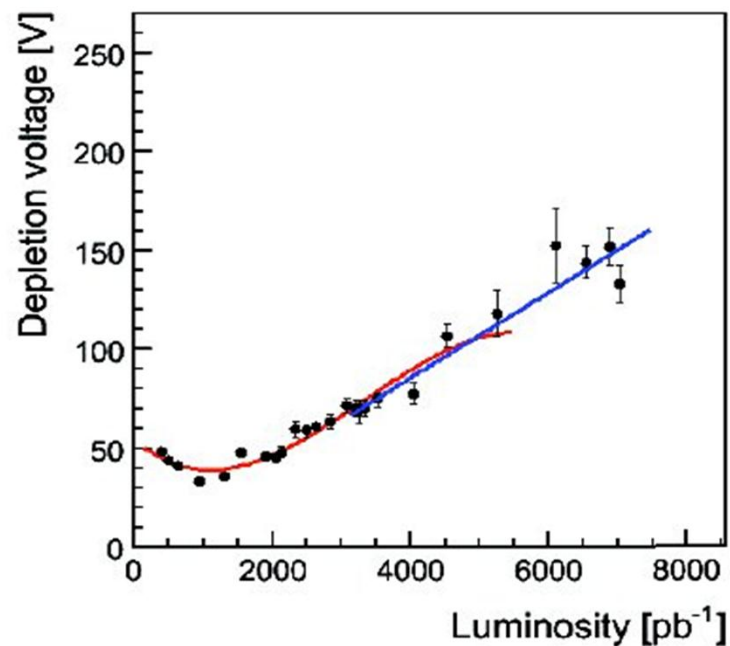
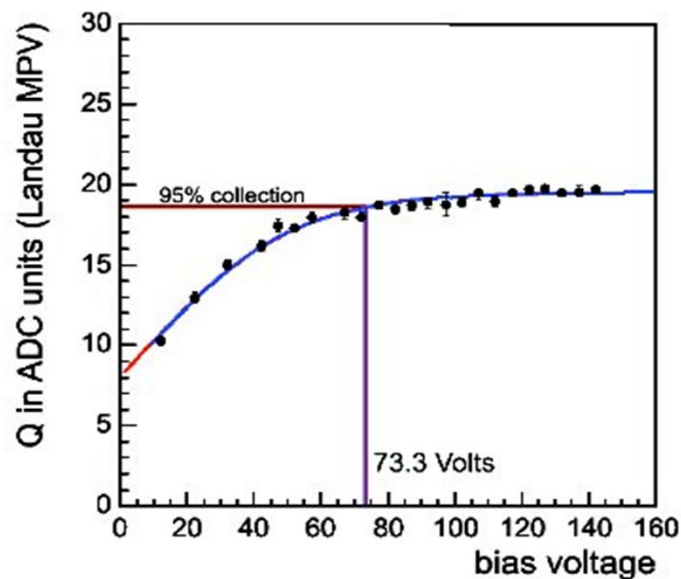


Fit signal charge (hits on tracks) to Landau \otimes Gaussian
Fit peak charge vs bias voltage to a sigmoid



Depletion Voltage study – Signal Vs. Bias

- Plot charge for different bias voltages
- Define depletion voltage, V_d , as voltage that collects 95% of the charge at the plateau

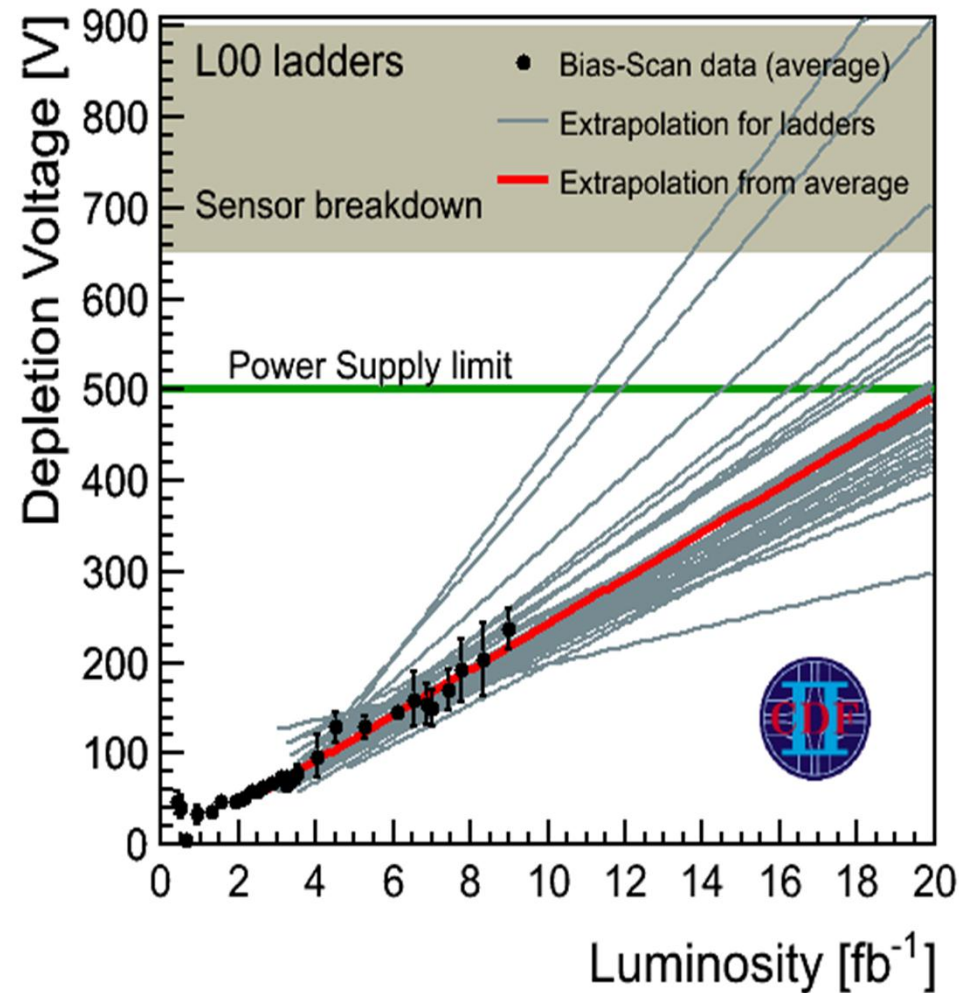


- Depletion Voltage as a function of integrated luminosity
3rd order polynomial fit around the inversion point
Linear fit to extrapolate to the future

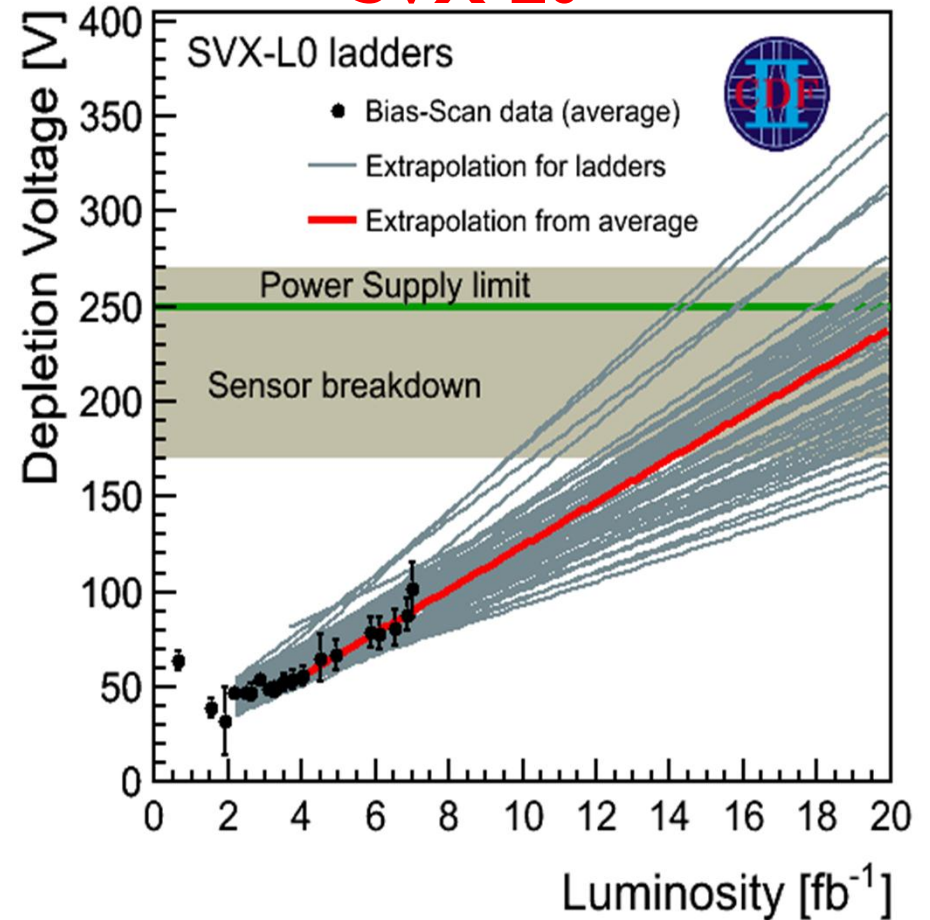


Depletion Voltage Projections L00-L0

Prediction for L00

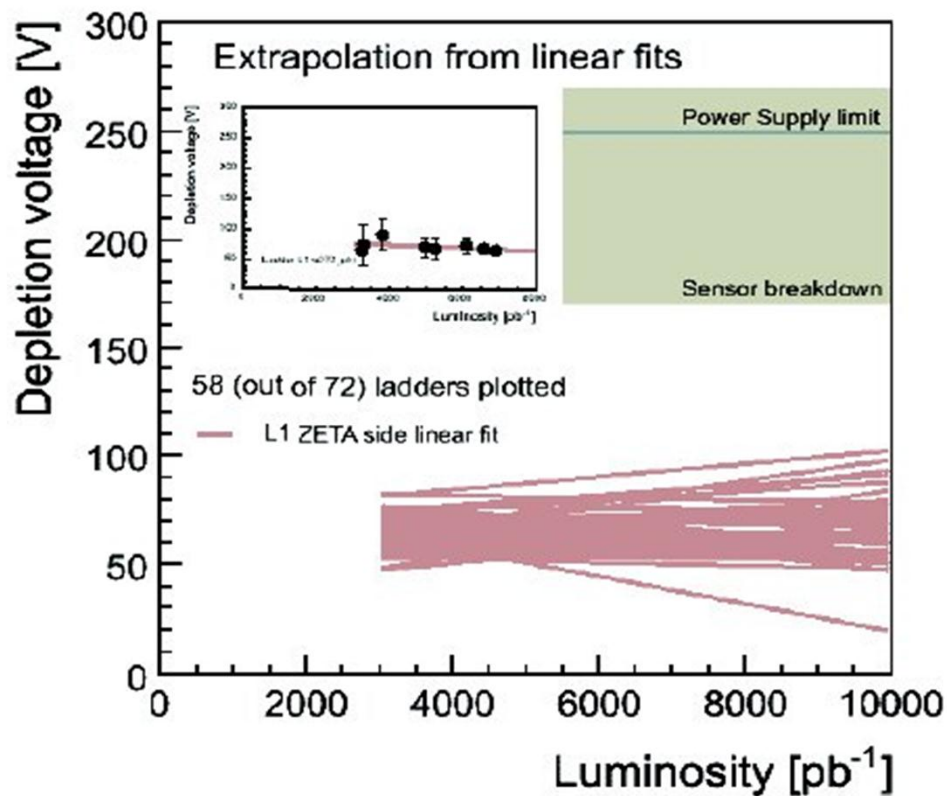
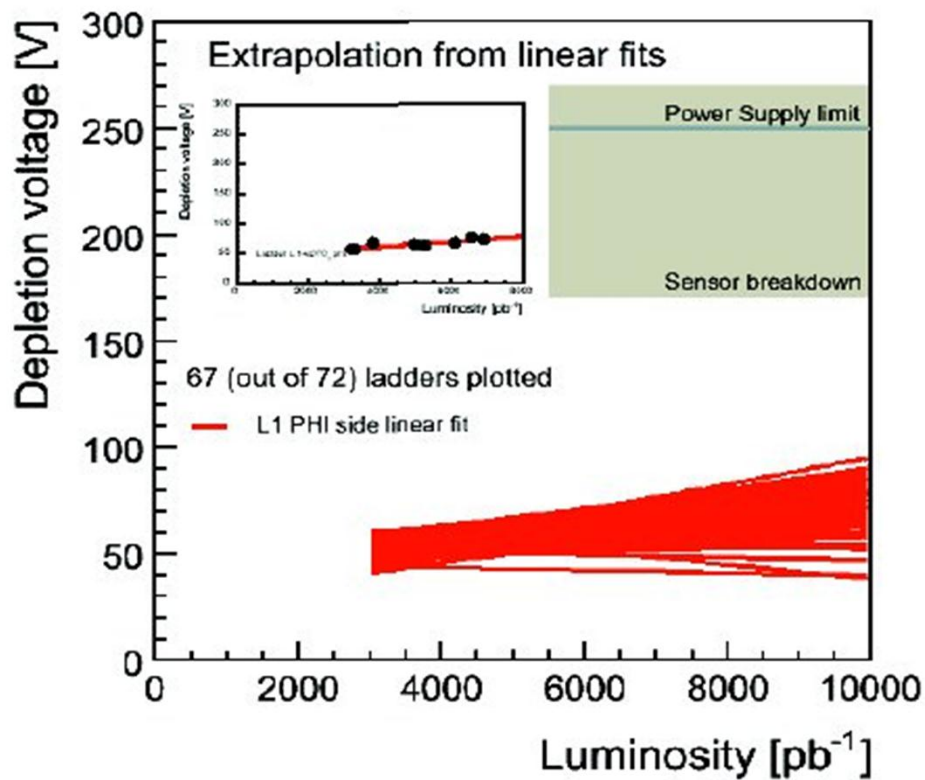


Prediction for SVX-L0





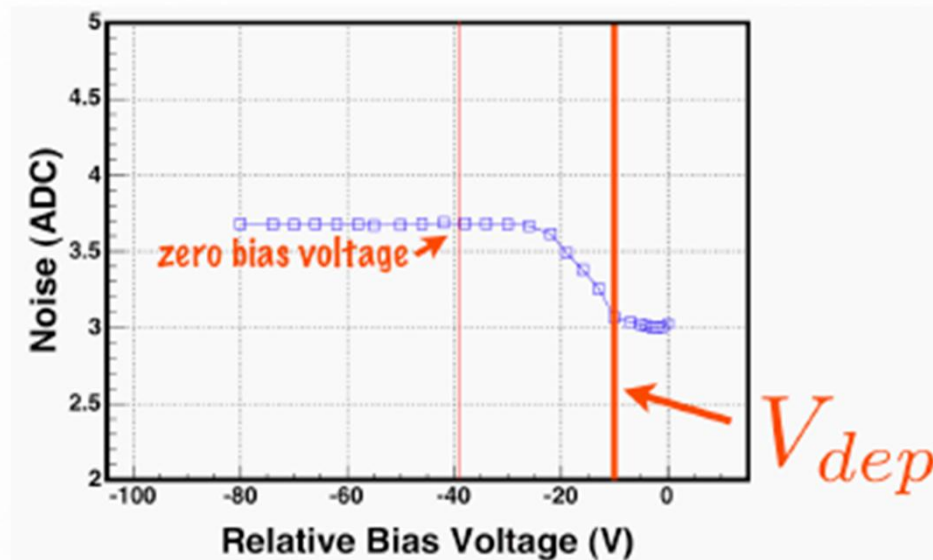
Depletion Voltage Projection L1





Depletion Voltage study Noise Vs. Bias

Noise vs Bias Method



Find average dnoise vs bias voltage

Depletion voltage taken as interpolation to 10⁴% of minimum value

GOOD: does not require beam time

BAD: not possible for single side strip or after inversion type

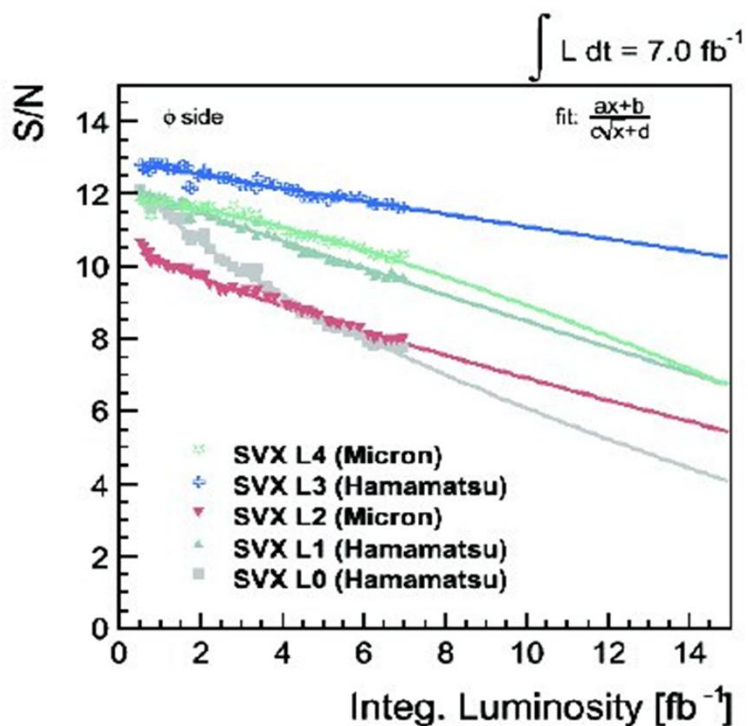


Signal / Noise projection

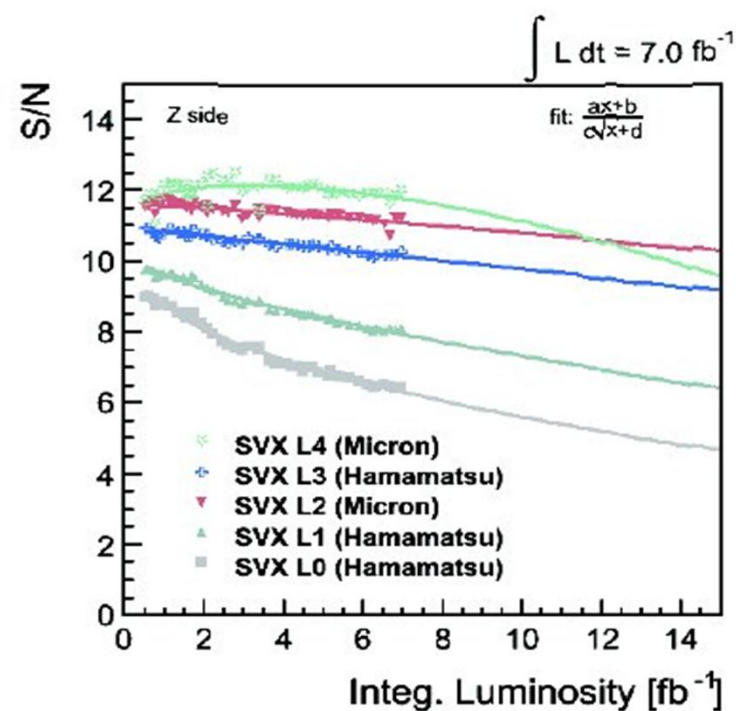
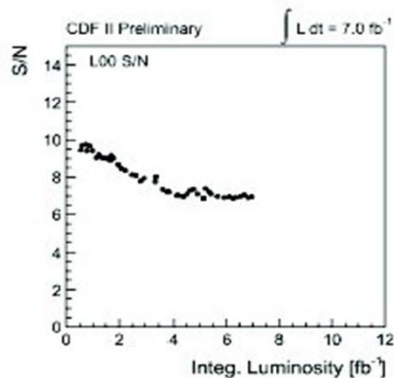
Signal from $J/\psi \rightarrow \mu^+\mu^-$ tracks strip cluster charge,
Noise estimation from regular calibrations

r-phi

z

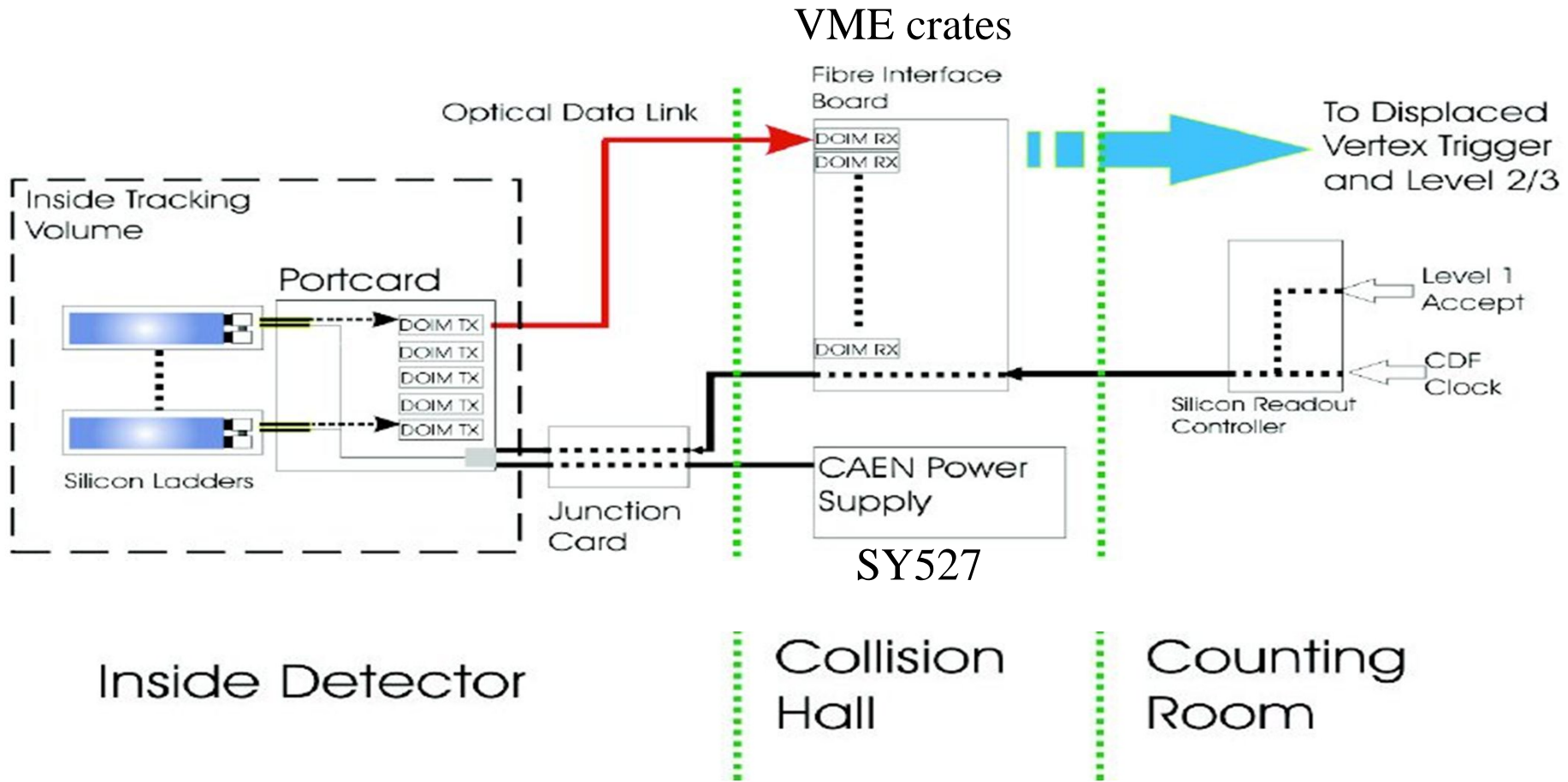


L00





Not only the sensors are in a radiation environment



Main components:

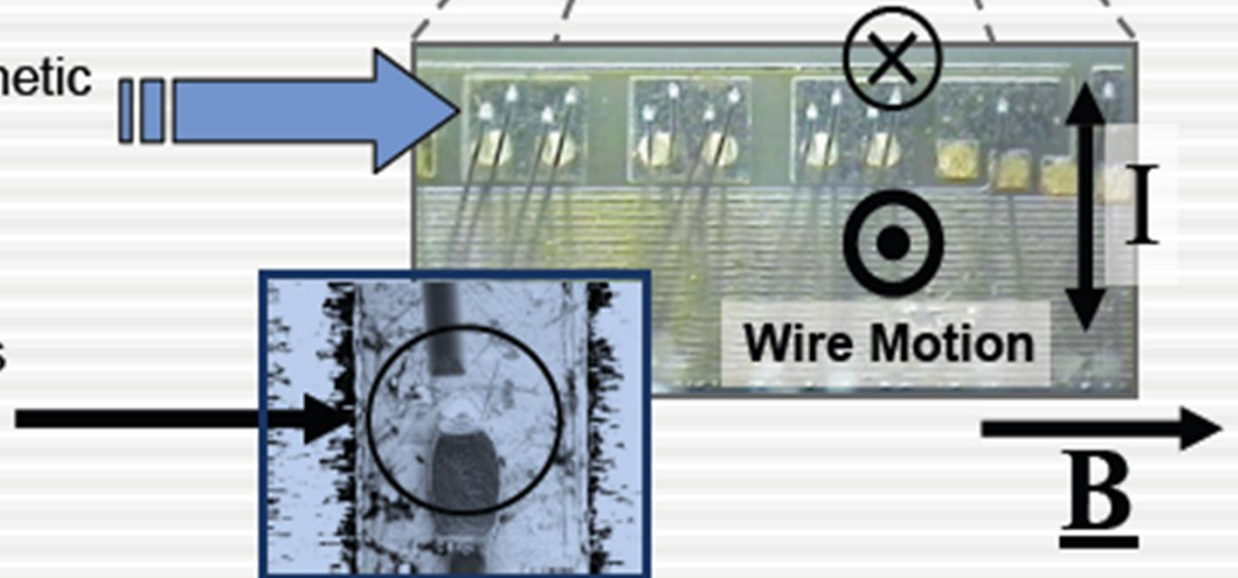
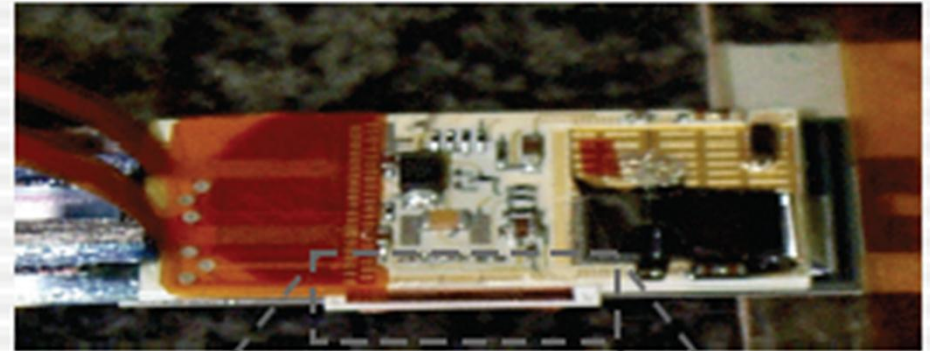
- Silicon Readout Controller (SRC):** "brain" of the system
- Fiber Interface Board (FIB):** control signals and optical readout
- Portcard:** chip commands and optical transmitters (DOIMs)



Problems induced by trigger rates:

Wirebond Resonances:

- Observed loss of data & power to z sides of ladders
 - Found to correlate with high trigger rates
- Failure due to wirebond resonances
 - Wires orthogonal to magnetic field
 - Wires feel Lorentz force during readout
 - If frequency is right, wires resonate and break



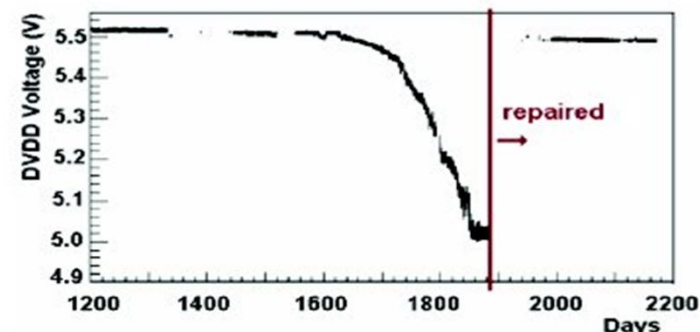


Other Operational Challenges

➤ CAEN SY527 Power Supplies

-Communication loss, corrupted read-back, spontaneous switch off,leaking capacitors

-A significant fraction of the supplies has been repaired

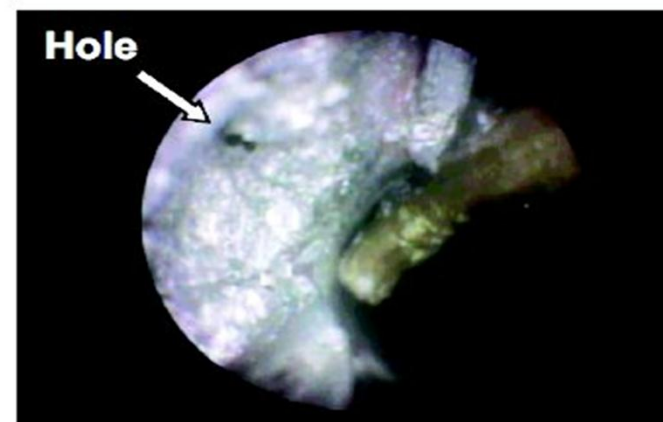


➤ ISL Cooling Repairs

-Glycol-water mix turned acidic causing corrosion.
-Repairs are challenging, access is possible only from inside the cooling conduits.

-Repairs during the 2007 and 2009 shutdowns have significantly improved the tightness of the system

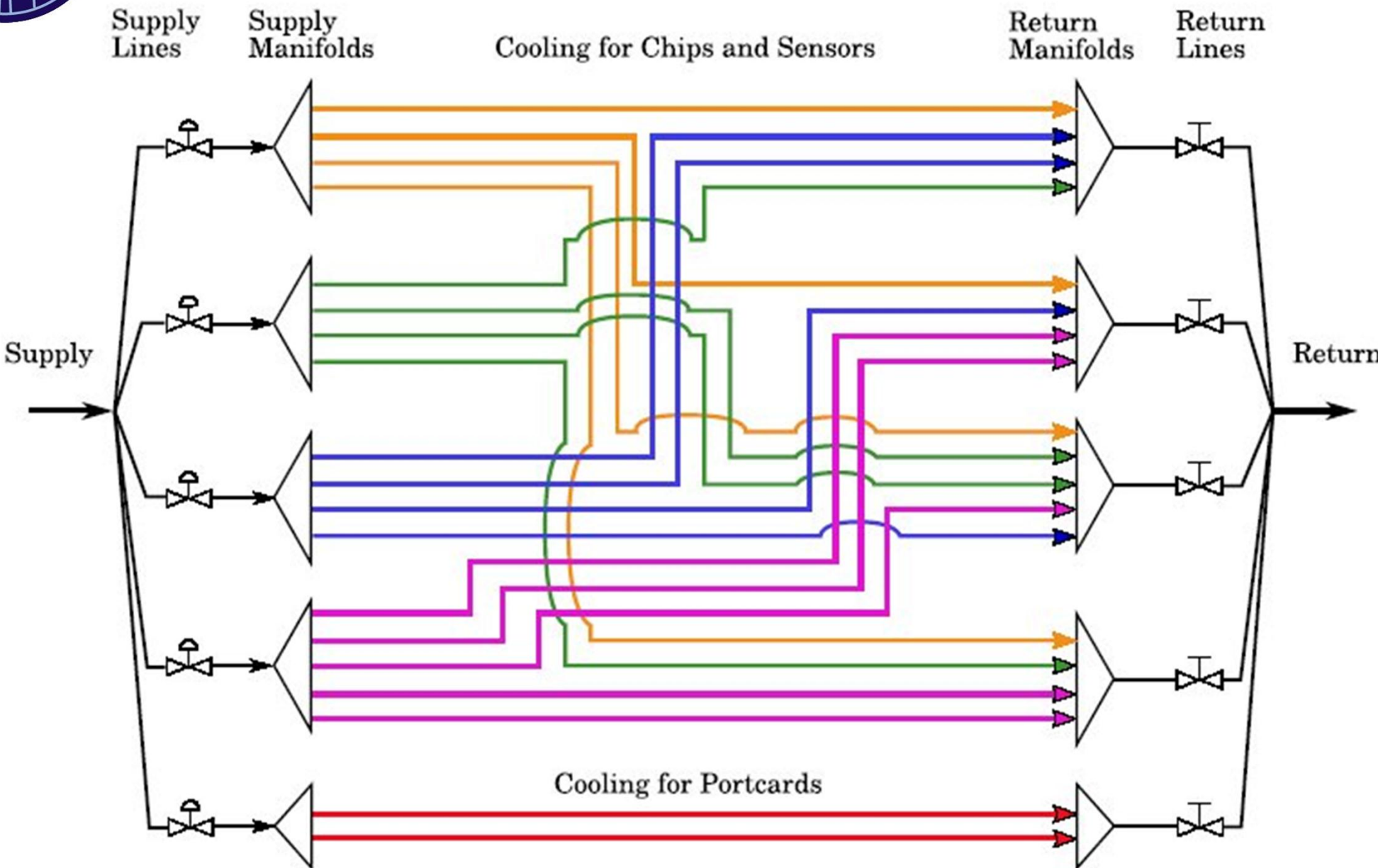
-Additional repairs to conical manifolds are planned for this summer



➤ Spare electronic components... etc.,etc.



ISL cooling lines



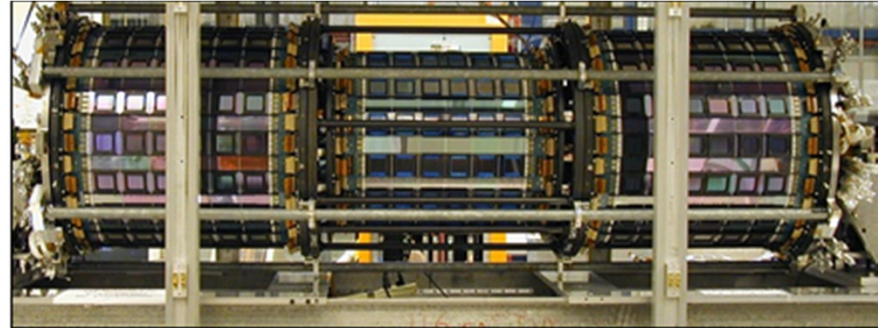
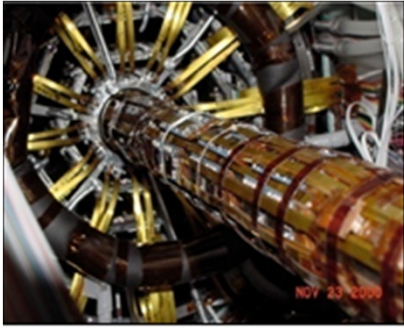


Conclusions

- The CDF Run II silicon detectors are in good health after 10 years of operation.
- The inner layers have long progressed through inversion and exhibit consistent post-inversion behavior.
- Most ladders in SVX-L0 and SVX-L1 layers and the rest of the detector are expected to be operable with high efficiency to 12 fb⁻¹.
- L0 will begin to be affected beyond that point, which does not affect our b-vertex detection efficiency significantly.

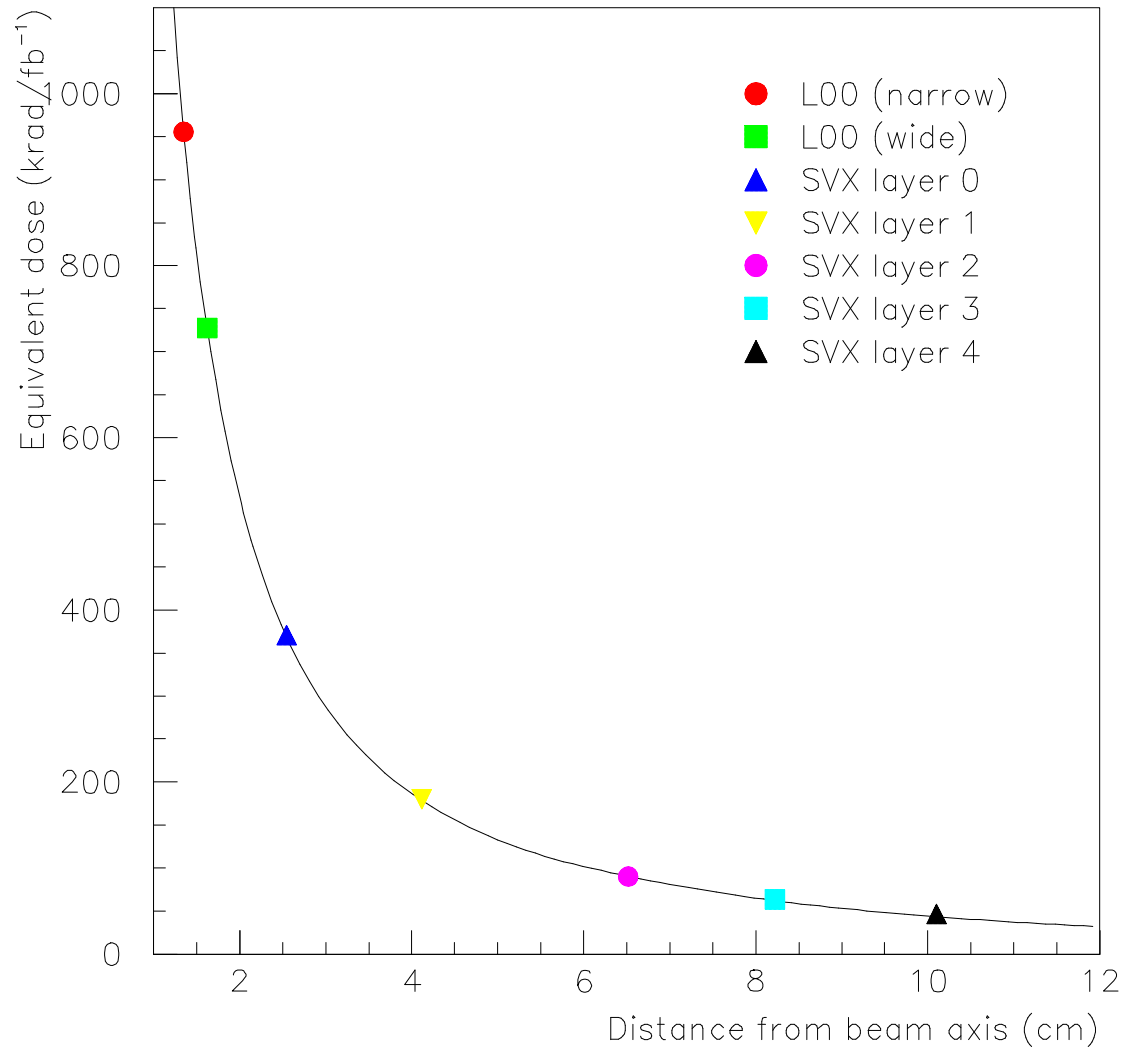


Back-up slides



Measured Radiation Field

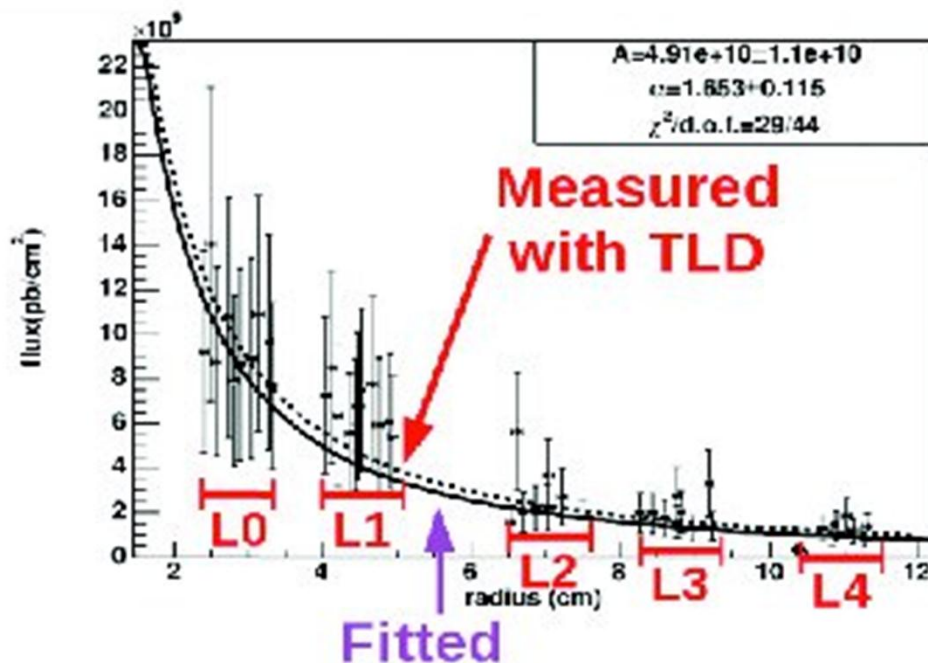
- Radiation field measured with TLDs outside the silicon volume in 2002-2003.
- NIM A514 188 (2003)
- Bias current evolution 2002-2004 consistent with this radiation dose





Evolution of Bias currents

- Fluence in the CDF detector volume is **dominated by the physics collisions** - related to the delivered luminosity. . Measured using TLDs (R. J. Tesarek et al. NSS 2003)
- The fluence – integrated luminosity relationship depends on distance of the sensor to the beam, and is computed by extracting the fluence from the change in bias current.
- Using a 95 pb^{-1} data sample collected in 2004, a damage factor of 1.65 ± 0.12 was extracted from bias current data (P. Dong et al. CDF/7275).
- Bias evolution and TLD measurements agree well





| | SVX II | ISL |
|--------------|---------|---------|
| Detectors | 720 | 900 |
| Half ladders | 360 | 300 |
| Chips | 3168 | 2100 |
| Channels | 405,504 | 268,800 |
| Hybrids | 720 | 300 |
| Port Cards | 72 | 30 |



Table 1: Summary of L00, SVXII and ISL basic parameters.

| Name | Radius (cm) | Orientation | manufacturer |
|----------------|-------------|--------------------|---------------------|
| L00 (narrow) | 1.35 | $r\phi$ | SGS Thomson, Micron |
| L00 (wide) | 1.62 | $r\phi$ | Hamamatsu |
| SVX L0 | 2.54 | $r\phi, z$ | Hamamatsu |
| SVX L1 | 4.12 | $r\phi, z$ | Hamamatsu |
| SVX L2 | 6.52 | $r\phi, 1.2^\circ$ | Micron |
| SVX L3 | 8.22 | $r\phi, z$ | Hamamatsu |
| SVX L4 | 10.10 | $r\phi, 1.2^\circ$ | Micron |
| ISL L6 Central | 22.00 | $r\phi, 1.2^\circ$ | Hamamatsu |
| ISL L6 Fwd/Bwd | 20.00 | $r\phi, 1.2^\circ$ | Hamamatsu |
| ISL L7 Fwd/Bwd | 28.00 | $r\phi, 1.2^\circ$ | Micron |



Laser diode/photo diode

| Laser Diode | |
|--|------------------------------|
| 1550nm InGaAsP/InP edge emitting laser diode | |
| Wavelength | 1550 nm nominal |
| Bias Current | 20 mA |
| Threshold Current | 10 mA |
| Optical Power | ≥ 200 mW coupled to fiber |
| Forward Voltage | 1 V |
| Operating Temperature | 0-40 (°C) |

Table 5.10: Characteristics of laser diode

| Photo Diode | |
|------------------------------------|-----------------|
| Description: InGaAs/InP planar PIN | |
| Sensitive Wavelength | 1000-1605 nm |
| Responsivity (A/W) | 0.9 @1550 nm |
| Dark Current (nA) | ≤ 1.5 @-5V 25°C |
| Capacitance (pf) | ≤ 4 |
| Breakdown Voltage | 15 V |
| Bandwidth (GHz) | 1.9 @3dB |
| Operating Temperature | 0-40 °C |

Table 5.11: Characteristics of photodiode

| Driver Chip | |
|-------------------|--|
| Input | Differential with common mode voltage $2.5 \pm 0.5 V$ and differential swing greater than 100 mV |
| Data rate | 53 MHz |
| Switching time | $t_r, t_f \leq 1.5 ns$ |
| Channel skew | < 1ns |
| Supply Voltage | 5 V |
| Control input | TTL signal to disable driver |
| Power dissipation | < 2.3 mW |

Table 5.12: Characteristics of driver circuit

| Receiver Chip | |
|------------------------|---------------------|
| Output | ECL |
| Data rate (MHz) | 53 |
| Switching time (ns) | $t_r, t_f \leq 2.0$ |
| Channel skew (ns) | < 1 |
| Supply Voltage (V) | 5 |
| Power dissipation (mW) | < 2.0 |

Table 5.13: Characteristics of receiver circuit



| Detector Parameter | SVX' | SVX II |
|--|---------------------------|-----------------------------------|
| Readout coordinates | $r-\phi$ | $r-\phi$; $r-z$ |
| Number of barrels | 2 | 3 |
| Number of layers per barrel | 4 | 5 |
| Number of wedges per barrel | 12 | 12 |
| Ladder length | 25.5 cm | 29.0 cm |
| Combined barrel length | 51.0 cm | 87.0 cm |
| Layer geometry | 3° tilt | staggered radii |
| Radius innermost layer | 3.0 cm | 2.44 cm |
| Radius outermost layer | 7.8 cm | 10.6 cm |
| $r-\phi$ readout pitch | 60;60;60;55 μm | 60;62;60;60;65 μm |
| $r-z$ readout pitch | absent | 141;125.5;60;141;65 μm |
| Length of readout channel ($r-\phi$) | 25.5 cm | 14.5 cm |
| $r-\phi$ readout chips per ladder | 2;3;4;6 | 4;6;10;12;14 |
| $r-z$ readout chips per ladder | absent | 4;6;10;8;14 |
| $r-\phi$ readout channels | 46,080 | 211,968 |
| $r-z$ readout channels | absent | 193,536 |
| Total number of channels | 46,080 | 405,504 |
| Total number of readout chips | 360 | 3168 |
| Total number of detectors | 288 | 720 |
| Total number of ladders | 96 | 180 |

Table 5.1: Comparison of SVX' and 5-layer SVX II.



ISL

| | Atlas | Atlas | L3 | L3 | Delphi | Delphi | ISL | ISL |
|----------------------------|-------|-------|-----|------|--------|--------|-------|-------|
| side | n | n | p | n | n | n | p | n |
| S/N | 11 | 17 | 15 | 15 | 12 | 21 | >12 | 12 |
| RP (μm) | 112 | 112 | 50 | 150 | 100 | 50 | 110 | 146 |
| SP (μm) | 56 | 56 | 25 | 50 | 100 | 50 | 55 | 73 |
| SP/ $\sqrt{12}$ | 16.0 | 16 | 7.2 | 14.4 | 28.0 | 14.4 | 16.0 | 21.0 |
| σ (μm) | 15.6 | 12.9 | 7.0 | 15.0 | 23.0 | 10.0 | <16.0 | <23.0 |

Table 6.2: Comparison to other silicon detectors with alternate strip readout.

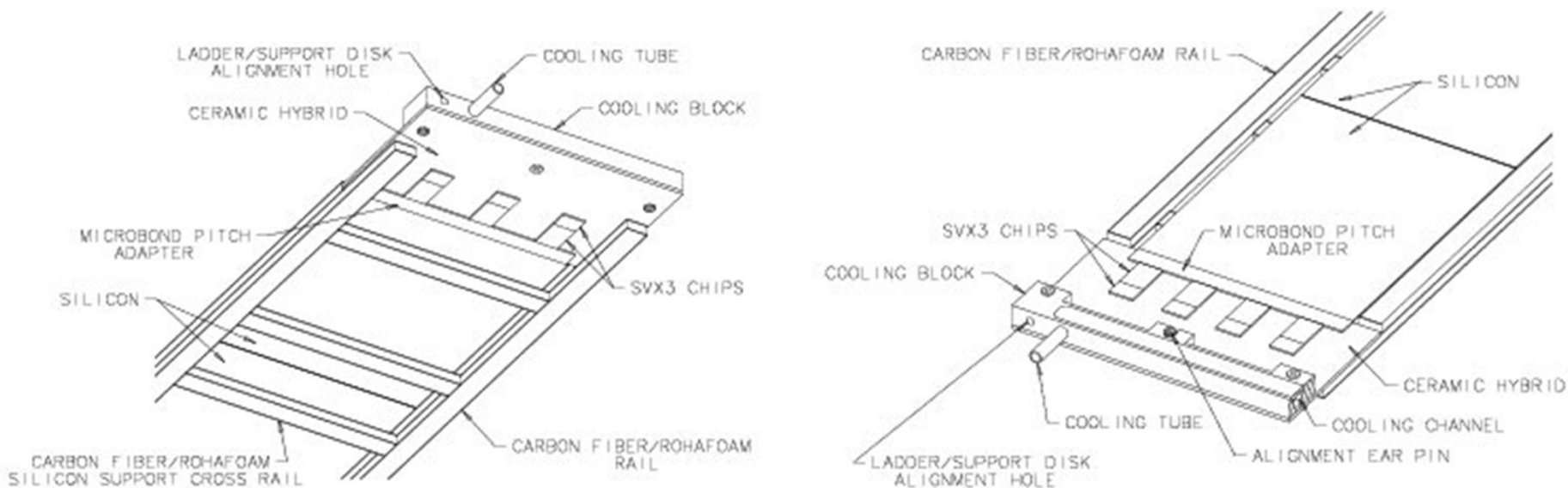


Figure 6.4: A close up view of the readout hybrid on the stereo side of a ladder (left) and the readout hybrid and cooling channel on the axial side of a ladder (right).

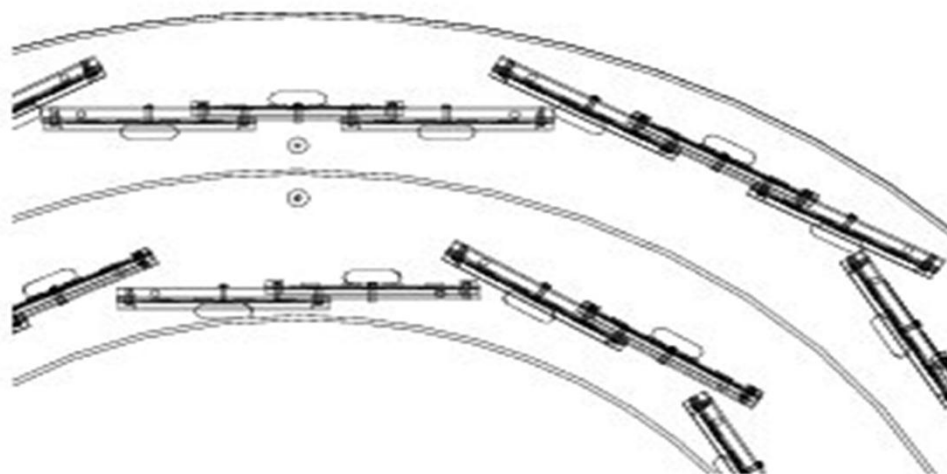


Figure 6.6: Closeup of one section of the end view of an endplug barrel.

ISL

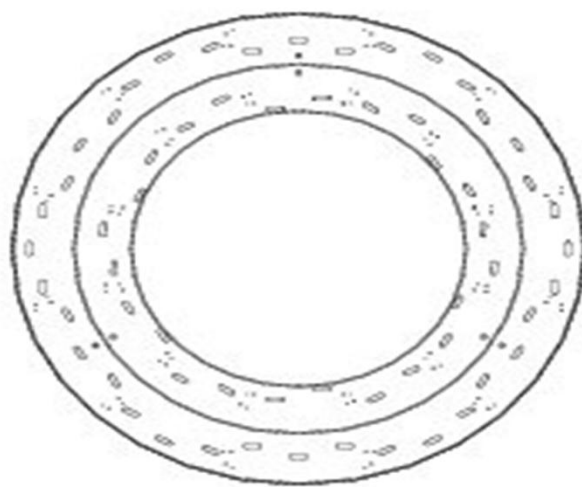


Figure 6.7: Carbon fiber support disks.

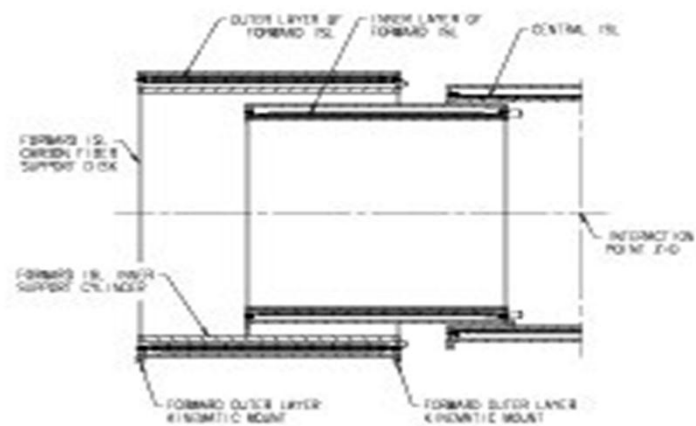


Figure 6.8: Schematic view of the ISL system.



Readout Chip Accounting

Some of the common failure modes:

- **Detector = Port-cards, Junction Cards, cables, and sensors issues.**
- **Optical = errors from the TX data transmitters in the port-cards**
- **Jumper failures = chip damage due to resonances**
- **AVDD2 = a SVX3D chip failure mode caused by thermal cycles**



END

This document was created with Win2PDF available at <http://www.win2pdf.com>.
The unregistered version of Win2PDF is for evaluation or non-commercial use only.
This page will not be added after purchasing Win2PDF.